의학박사 학위논문

The role of nArgBP2 in regulating the morphology of dendritic spine and the formation of excitatory synapses

수상돌기가시 형태와 흥분성 시냅스 형성을 조절하는 nArgBP2의 역할에 관한 연구

2019 년 8 월

서울대학교 대학원

의과학과 생리학/신경과학 전공

이 상 은

A thesis of the Degree of Doctor of Philosophy

수상돌기가시 형태와 흥분성 시냅스 형성을 조절하는 nArgBP2의 역할에 관한 연구

The role of nArgBP2 in regulating the morphology of dendritic spine and the formation of excitatory synapses

August 2019

The Department of Biomedical Sciences

Seoul National University College of Medicine

Sang-Eun Lee

수상돌기가시 형태와 흥분성 시냅스 형성을 조절하는 nArgBP2의 역할에 관한 연구

지도교수 장 성 호

이 논문을 의학박사 학위논문으로 제출함

2019 년 4 월

서울대학교 대학원

의과학과 생리학/신경과학 전공

이 상 은

이상은의 박사 학위논문을 인준함

2019 년 7 월

위 원 장 서 인수 (인)

부 위 원 장 장 성호 (인)

위 원 이 용석 (인)

위 원 최 형진 (인)

위 원 한 기흔 (인)

The role of nArgBP2 in regulating the morphology of dendritic spine and the formation of excitatory synapses

by

Sang-Eun Lee

A thesis submitted to the Department of Biomedical Sciences in partial fulfillment of the requirements for the Degree of Doctor of Philosophy in Medical Sciences at Seoul National University College of Medicine

July, 2019

Approved by Thesis Committee:

Professor _____ Chairman

Professor _____ Vice chairman

Professor _____

Professor _____

Professor _____

ABSTRACT

Dendritic spines are small postsynaptic protrusions on a dendrite that receive most of the excitatory synaptic input in the brain. The cytoskeleton of the dendritic spines is predominately composed of actin filaments which form the structural and functional network associating specialized substructures like postsynaptic density (PSD). The morphology of spines is highly variable and dynamically regulated with neuronal activity by actin-regulating proteins in PSD.

An increasing number of postsynaptic proteins such as SAPAPs and SHANKs are implicated in different forms of mood disorders such as bipolar disorders, autism spectrum disorders, obsessive-compulsive disorders, and schizophrenia although their underlying mechanisms have not been fully understood. Accumulating evidence from recent studies suggests that the structural remodeling of dendritic spines is critical for synaptic plasticity and the mechanisms regulating actin cytoskeleton may contribute to spine pathology in these neuropsychiatric disorders.

nArgBP2 was originally identified as a protein that directly interacts with SAPAP3, and. the previous study found that ArgBP2/nArgBP2 controls the balance between adhesion and motility by coordinating multiple signaling pathways converging on the actin cytoskeleton. A recent study

found that genetic deletion of ArgBP2/nArgBP2 (SORBS2) in mice is known to cause behavioral phenotypes resembling human intellectual disability (ID). It has been, however, mostly unknown that how nArgBP2 deficiency leads to phenotypes observed in ID and more importantly, how nArgBP2 functions at postsynapses and its relevance to the underlying cellular and molecular mechanisms that might be related to ID.

To investigate the roles of nArgBP2 at synapses, based on the results from previous studies, I set up the following research hypotheses in my dissertation. 1) nArgBP2 is one of the key protein that regulates actin cytoskeleton at postsynapses, 2) nArgBP2 regulates the morphological changes of dendritic spines, 3) given that dendritic spines are major sites that receive most of the excitatory synaptic inputs, nArgBP2 controls the formation of excitatory synapses, 4) since excitatory–inhibitory synaptic balance(E/I balance) is the key mechanism that maintains homeostatic functional properties of nervous system, E/I imbalance caused by nArgBP2 deficiency might be the underlying factor associated with synaptic dysfunction observed in ID.

I found that the knockdown (KD) of nArgBP2 by specific shRNA resulted in a dramatic change in dendritic spine morphology. The nArgBP2 KD also impaired the formation of excitatory synapses which largely

terminated at dendritic shafts instead of dendritic spine heads in spiny neurons. The aberrant formation of excitatory synapses resulted in a reduced mean frequency of miniature excitatory postsynaptic currents. I also found that the morphological changes were associated with increased WAVE1/PAK/cofilin phosphorylation, and this effect was rescued by either inhibiting PAK or activating cofilin combined to sequestration of WAVE. Using live-cell imaging technique, I confirmed that a marked increase of actin cytoskeleton dynamics resulted in a significant increase in the motility of dendritic spines in nArgBP2 KD neurons.

Surprisingly, nArgBP2 KD did not cause any morphological defect in the mature stage when the dendritic spines were stabilized. I inferred that nArgBP2 may be needed when significant structural remodeling is needed, such as developing stage. To test this idea, I decided to induce chemically-induced Long Term Potentiation (cLTP) in mature neurons. It is known to mimic many features of developing stages, including dramatic remodeling of pre-and postsynaptic structures in mature neurons. The cLTP significantly increased the size of the spine heads of control neurons while remained almost the same in nArgBP2 KD neurons. I also measured the 3D morphological features of dendritic spines under the same conditions and found that cLTP in nArgBP2 KD neurons could not induce normal head enlargement in dendritic spines. These results

support my idea that nArgBP2 controls the actin cytoskeleton dynamics also in mature neurons.

Together, my research suggests that nArgBP2 functions to regulate the actin cytoskeleton dynamics in dendritic spines. It plays a particularly important role when active structural remodeling is needed, such as spine morphogenesis and subsequent spine–synapse formation in developing stages and during synaptic plasticity in mature stages. The results also raise the possibility that the aberrant regulation of synaptic actin dynamics caused by reduced nArgBP2 expression may contribute to the synaptic excitatory/inhibitory imbalance observed in ID.

* This work is published in *PNAS* (1) .

.....

Keywords: nArgBP2, dendritic spines, actin cytoskeleton, excitatory synapse, chemical long–term potentiation, excitatory/inhibitory balance,
Student Number : 2013–23532

CONTENTS

List of Figures and Tables

List of Abbreviations

cLTP: chemical long-term potentiation

DIV: Days *in vitro*

FRAP: fluorescence recovery after photobleaching

KD: Knockdown

LIMK: LIM-domain containing protein kinase

mEPSC: miniature excitatory postsynaptic currents

mIPSC: miniature inhibitory postsynaptic currents

nArgBP2: neural Abelson-related gene binding protein 2

PAK: p21-activated kinase

SAPAP: synapse-associated protein 90/postsynaptic density protein 95-associated protein

shRNA: small hairpin RNA

SIM: structured illumination microscopy

vGAT: vesicular GABA transporter

vGLUT1: vesicular glutamate transporter 1

WASP: Wiskott-Aldrich syndrome protein

WAVE: WASP-family verprolin-homologous protein

INTRODUCTION

The postsynaptic enriched adaptor protein nArgBP2 (neural Abelson-related gene binding protein 2), which represents a neural specific splice variant of the ubiquitous ArgBP2, was originally identified as a binding partner of synapse-associated protein 90/postsynaptic density protein 95-associated protein 3 (SAPAP3) (2). It belongs to a family of adaptor proteins that are involved in the regulation of cell adhesion, actin cytoskeleton organization, and signaling downstream of growth factor receptors (3). This protein family is characterized by a sorbin homology (SoHo) domain in the NH_2-terminal region and three SH3 domains in the COOH-terminal region (4). While the SoHo domain remains poorly characterized, the SH3 domains bind signaling protein kinases, such as Abl, Arg and Pyk2; the ubiquitin ligase Cbl; and protein involved in the regulation of focal adhesions and adhering junctions, such as vinculin and Afadin (2, 5-7). It was previously reported that the NH_2-terminal region of nArgBP2, which contains the SoHo domain, interacts with spectrin, while the COOH-terminal SH3 domains bind dynamin, synaptojanin, Wiskott-Aldrich syndrome protein (WASP)-family verprolin-homologous protein (WAVE) isoforms, and WAVE regulatory proteins (4), all of which participate in the regulation of the actin cytoskeleton (Figure 1). It was also found that the downregulation of both ArgBP2 and nArgBP2 expression in astrocytes redistributes focal adhesion proteins

and increases peripheral actin ruffles (4), whereas nArgBP2 overexpression causes a coalescence of the actin cytoskeleton, suggesting that nArgBP2 controls the balance between adhesion and motility by coordinating actin cytoskeleton dynamics.

Key players in the regulation of actin dynamics are WAVE and Rac1 proteins. WAVE regulates actin-dependent processes by activating the actin-related protein (Arp2/3) complex (8). Phosphorylation of WAVE1 by cyclin-dependent kinase 5 is known to regulate actin polymerization and dendritic spine morphology (9). Rac1 also regulates dendrite initiation, elongation, and the complexity of branching as well as spine formation (10, 11). The major downstream effector of Rac1 is p21-activated kinase (PAK) that controls LIM-domain containing protein kinase (LIMK), which in turn facilitates actin filament stabilization through the phosphorylation and inactivation of the actin depolymerizing factor cofilin (12-15). Aberrant WAVE/Rac1/PAK signaling leads to abnormal actin regulation that causes defects in neuronal connectivity and synaptic plasticity (16, 17). Importantly, genetic analyses have revealed that mutations in genes regulating actin filament network at glutamatergic synapses are associated with intellectual disability (ID) (18), autism (19), and schizophrenia (SCZ) (20), indicating dysregulation of actin cytoskeleton as one common pathophysiological mechanism for these disorders.

nArgBP2 mRNA is highly expressed in isocortex, hippocampal formation, cortical subplate, striatum, thalamus and hypothalamus (21), majority of which are regions of the brain associated with bipolar disorder (BD) (22). Furthermore, genetic deletion of nArgBP2 in mice leads to behavioral phenotypes such as increased activity, compulsive/repetitive risk-taking and hedonistic behaviors that resemble many symptoms of ID and BD (23, 24). Recent study showed that genetic deletion of SAPAP3, a binding partner of nArgBP2, causes repetitive grooming and anxiety-like behaviors in mice, thus implicating it in the pathogenesis of obsessive-compulsive behaviors(25). Another latest study have shown overexpressed Shank3 causes manic-like behaviors in both humans and mice (26), while loss of Shank3 is linked to autism spectrum disorders through previous studies of human genetics and knockout mice (27, 28). Interestingly, Shank3 binds to SAPAP/GKAP that interact directly with nArgBP2, again positioning nArgBP2 as a hub in the etiology of various mood disorders. Despite the high possibility that nArgBP2 could be involved in the etiology of such mood disorders, remarkably none is known about the role of nArgBP2 at synapses or its connection with the synaptic dysfunctions associated to these neurological disorders.

In this study, I found that the nArgBP2 KD causes a dramatic change in spine morphology and a robust inhibition of excitatory spine-synapse

formation. In particular, I observed that nArgBP2 downregulation increases actin dynamics through the activation of Rac1/WAVE/PAK pathway, which flows into the decrease of cofilin activity. I also observed that in mature neurons, nArgBP2 has a role in synaptic structural plasticity which also involves regulation of actin dynamics. Thus, I provide evidence that nArgBP2 regulates spine morphogenesis and subsequent spine–synapse formation at glutamatergic synapse by controlling actin dynamics.

Since recent reports have showed as genetic deletion of nArgBP2 in mice leads to ID and manic/bipolar–like behavior, my results shed new light on the underlying mechanism for the synaptic dysfunction caused by nArgBP2 downregulation that may associate with analogous human neurological disorder.

MATERIALS AND METHODS

Animal experimental procedures were approved by the Institute of Animal Care and Use Committee (IACUC, Approval ID number: SNU-100930-5) of Seoul National University, Korea. All experiments were carried out in accordance with the approved guidelines and regulations.

DNA constructs and reagents

Full-length HA-tagged rat nArgBP2 cDNA (amino acids 1-1196) was constructed as previously described (4). GFP-tagged nArgBP2 was manipulated by subcloning the full-length sequence in pEGFPC1 by PCR. GFP-actin was kindly provided by Gilbert Di Paolo (Columbia University, New York, NY). Full length cDNA encoding rat myc-tagged nArgBP2 was digested to generate a cDNA fragment encoding a truncation of nArgBP2 (a.a.1-867) devoid of the SH3 domains (nArgBP2 Δ-SH3) and was subcloned in pEGFP-C2. The first and second SH3 domains of nArgBP2 (a.a. 959-1110) or the third on its own (a.a. 1137-1195) were PCR amplified and were subcloned upstream of the GFP cDNA fused to the mitochondria localization signal of OMP-25 (last 27 a.a.) (named mSH3-1/2 or mSH3-3). The fidelity of all constructs was verified by DNA sequencing. NSC23766 was from Tocris Biosciences (Bristol, UK). All other reagents were from Sigma (St. Louis, MO).

RNA-mediated interference and rescue experiments

RNA interference (RNAi)-mediated nArgBP2 knockdown was carried out by expressing small hairpin RNA (shRNA) duplexes through pU6 expression vector. The targeted sequence of rat nArgBP2 from its cDNA sequence (Gene bank accession number NM_O35413) was 5' - GGACTGGTACAAGACAATGTT -3' (nucleotides 585-605)(4) common to human nArgBP2 cDNA sequence. In particular, this target sequence is also present in all eight isoforms of ArgBP2. To exclude artificial effects of the expression vector, a scrambled sequence of the forward primer was designed; 5' - GGCGAAATACATAGTGTGACT - 3' (http://www.sirnawizard.com/). A pair of complementary oligonucleotides was synthesized separately with the addition of an BamHI enzyme site at the 5′ end and an EcoRI site at the 3′ end. The annealed cDNA fragment was cloned into the BamHI-EcoRI sites of RNAi-Ready pSIREN-DNR-DsRed vector (Clontech Laboratories, Mountain View, CA). All constructs were verified by sequencing. After transfection, cells were cultured for over 72 h. For evading RNA interference, silent mutations within shRNA targeting sequence (C593T, G596A, and A599G) in GFP-nArgBP2 and GFP-⊿SH3-nArgBP2 were generated using the QuikChange Site-Directed Mutagenesis Kit (Stratagene, La Jolla, CA). The fidelity of all constructs was verified by sequencing. KD efficiency was examined in GFP-nArgBP2-expressed

HEK293T cells or AAV-shRNA-infected cultured cortical neurons by Western blotting.

Production of adeno-associated virus

shRNA or scrambled sequences was cloned into the adeno-associated virus vector (pAAV-U6-GFP-shRNA) using BamHI/SalI sites. For electrophysiology, we used pAAV-U6-GFP-shRNA-nArgBP2 or scrambled vector as a transient transfection vector. For AAV production, vectors were co-transfected with the pAAV-RC1 and pHelper vector in the 293T packaging cell line (Cell Biolabs, San Diego, CA). 48-72 h after transfection, cells were harvested and AAVs were purified by ultracentrifugation as previously described (29). Genomic titers were determined using the StepOne™ Real-Time PCR Systems (Applied Biosystems, Foster City, CA) with primers designed to GFP. 10 μl (1.0 X 10^{12} GC/ml) of purified AAV virus were treated to cultured cortical neurons at DIV 6 and used at DIV 21.

Cell culture and transfection

HEK293T and HeLa cells were cultured at 37℃ and 5 % CO_2 in DMEM (Invitrogen, Carlsbad, CA) supplemented with 10 % fetal bovine serum

and transfected with GFP-nArgBP2 and shRNAs using Lipofectamine 2000 (Invitrogen). Cells were examined for transfection efficiency after 16-24 h under a fluorescence microscope.

Western blot

HEK293T cells or AAV-infected cortical neurons were lysed with RIPA buffer (20 mM Tris, pH 7.5, 100 mM NaCl, 50 mM NaF, 0.1 % DOC, 1.0 % SDS, 1 mM orthovanadate) in the presence of a protease inhibitor cocktail (Roche, Mannheim, Germany), clarified by centrifugation 15,000 × g for 10 min, and incubated for 15 min in 37℃ water bath. Protein concentrations were measured with a Bicinchoninic acid protein assay reagent kit (ThermoFisher, Waltham, MA). Samples containing 50 μg of total protein were separated by SDS-PAGE and transferred to PVDF membranes (Pall Life Science, Ann Arbor, MI). The membranes were blocked for 1 h with 5 % nonfat dry milk in TBST (10 mm Tris-HCl, pH 7.6,100 mm NaCl, and 0.1 % Tween 20) incubated with the respective primary antibodies for 2 h at room temperature or overnight at 4℃. After extensive washing in TBST, the membrane was incubated with corresponding HRP-conjugated secondary antibody for 1 h. Chemiluminescence reactions were performed with AbSignal Western detection kit system (AbClon, Seoul, South Korea) and acquired using an

ImageQuant LAS 4000 (GE Healthcare, Uppsala, Sweden); images were analyzed by the ImageJ software.

Antibodies

Rabbit polyclonal anti-nArgBP2 antibody was originally raised from De Camilli Laboratory (Yale University, New Haven, CT) and rabbit polyclonal anti-GFP antibody was produced by our lab. Mouse monoclonal anti-nArgBP2 antibody was purchased from Sigma. Rabbit polyclonal anti-PAK1+2+3 antibody, rabbit monoclonal anti-phospho PAK1+2+3 antibody and Mouse polyclonal anti-β-tubulin was purchased from Abcam (Cambridge, UK). Mouse monoclonal HA antibody was purchased from Covance (Princeton, SN). Rabbit polyclonal anti-WAVE1 antibody and anti-phospho-WAVE1 antibody was purchased from ECM Biosciences (Versailles, KY). Rabbit polyclonal anti-cofilin antibody and phospho-cofilin antibody was from Cell Signaling technology (Danvers, MA). Rabbit polyclonal anti-VGAT, rabbit polyclonal anti-vGlut1, mouse monoclonal anti-GAD1(GAD67), mouse monoclonal anti-PSD95 and mouse monoclonal anti-gephyrin were from Synaptic Systems (Göttingen, Germany). Mouse monoclonal anti-Flag (M2), rabbit polyclonal anti-Flag and anti-p32 were from Sigma. HRP-

conjugated anti-rabbit or anti-mouse Secondary antibodies were from Jackson ImmunoResearch (West Grove, PA).

Primary Neuron culture and Transfection

Primary rat hippocampal or cortical neurons derived from embryonic day 18 Sprague Dawley fetal rats of either sex were prepared as described previously (30). Briefly, hippocampi or prefrontal cortexes were dissected, dissociated with papain, and triturated with a polished half-bore Pasteur pipette. 2.5 x 10^5 cells resuspended in minimum Eagle's medium (Invitrogen) supplemented with 0.6 % glucose, 1mM pyruvate, 2 mM L-glutamine, 10% fetal bovine serum (Hyclone, South Logan, UT), were plated on poly-D-lysine-coated glass coverslips in a 60 mm Petri dish. Four hours after plating, the medium was replaced with neurobasal medium (Invitrogen) supplemented with 2 % NS21, 0.5 mM L-glutamine. 4 mM 1-beta-D-cytosine-arabinofuranoside (Ara-C; Sigma) was added as needed. 5.0 x 10^6 cortical neurons derived from prefrontal cortexes were plated on poly-D-lysine-coated 100 mm Culture dish. Neurons were transfected using a modified calcium-phosphate method (3). Briefly, 6 μg of DNA and 18.6 μl of 1M $CaCl_2$ were mixed in distilled water to a total volume of 75 μl and the same volume of 2xBBS was added. The cell culture medium was completely replaced by transfection medium

(MEM; 1 mM pyruvate, 0.6 % glucose, 10 mM glutamine, and 10 mM HEPES, pH 7.65), and the DNA mixture was added to the cells and incubated in a 5 % CO2 incubator for 60 min. Cells were washed twice with washing medium, pH 7.35, and then returned to the original culture medium. Neurons were co-transfected at DIV 9 and fixed at DIV 16. Co-transfection was performed at a ratio of 1:2. For triple-transfection, GFP-tagged mSH3-1/2 or mSH3-3, DsRed-tagged-shRNA-nArgBP2, and HA-tagged PID or S3A constructs were used at a ratio of 1:1:1. Neurons coexpressing mSH3-1/2(-3) and shRNA-nArgBP2 were identified by red and green fluorescent signals, and PID or S3A expression was confirmed by retrospective HA-immunostaining. Only neurons positive for all three signals were included in analysis.

Immunocytochemistry

Cultured neurons were fixed in 4 % paraformaldehyde, 4 % sucrose, PBS for 15 min at RT and subsequently permeabilized with 0.25 % Triton X-100 in PBS for 3 min at RT or in 100 % Methanol at -20℃ for 5 min. Neurons were then blocked with 10 % normal goat serum in PBS for 1 hour at RT. Primary antibodies diluted in 3% normal goat serum in PBS were added and incubated for 2 h at RT. Secondary antibodies (Invitrogen) were diluted 1:2000 in 3 % normal goat serum in PBS and incubated for

1 h at RT. The primary antibodies were diluted and used at the following dilutions: Rabbit polyclonal anti-nArgBP2 1:500, mouse monoclonal anti-nArgBP2 1:500 Mouse monoclonal HA 1:250, Rabbit polyclonal anti-VGAT 1:5000, rabbit polyclonal anti-vGlut1 1:5000, mouse monoclonal anti-GAD1(GAD67) 1:500, mouse monoclonal anti-PSD95 1:500 and mouse monoclonal anti-gephyrin 1:500

Image acquisition and quantitative analysis

Immunofluorescence labeled cells were mounted and analyzed using a Zeiss fluorescence microscope, a 40X oil-immersion lens (1.25 NA), an EMCCD camera (iXon887, Andor Technologies, Belfast, Northern Ireland) and MetaMorph Imaging software (Universal Imaging Corporation, West Chester, PA). For analysis, well branched pyramidal or multipolar neurons were randomly selected, and the experiments were performed in a blinded manner. Mushroom spines were defined as dendritic protrusions of around 1 μm in length and with a head of width > 0.6 μm, while filopodia as protrusions of at least 3 μm in length, but without head. Spine head was defined as the tip structure at least 1.3 times thicker than the spine neck. The numbers of dendritic spines and filopodia were counted manually to estimate the density (number of protrusions per 50 μm length of the primary or secondary dendritic branches). Statistical

significance was analyzed using Student's t-test where $p < 0.05$ was set as the minimum value of significance. For multiple conditions, I compared means by ANOVA followed by Tukey's HSD post hoc test.

The numbers of dendritic spines were described as mean ± SEM (at least three-independent experiments). Outlines of spine heads were created from thresholded images using edge-detection functions of Metamorph.

Manders' colocalization coefficients (MCC) were calculated using Image J with JACoP plug-in function (http://rsbweb.nih.gov/ij). Region of Interests (ROIs) were first selected from the merged RGB images, and color-separated into green (PSD95/gephyrin) and red (nArgBP2) channels. Background was automatically identified using Costes threshold regression before MCC calculation (31).

Live cell imaging and FRAP (fluorescence recovery after photobleaching) analysis

For live cell imaging, the culture medium was replaced with pre-warmed Tyrode's solution (119 mM NaCl, 2.5 mM KCl, 2 mM $CaCl_2$, 2 mM $MgCl_2$, 25 mM HEPES, pH 7.4 and 30 mM glucose). Experiments were performed using a stimulus setting menu in OLYMPUS FLUOVIEW to

control sequential image acquisition using a 100X oil-immersion lens (1.40 NA) equipped with a FV-1000 confocal microscope (Olympus, Tokyo, Japan) to accomplish photobleaching of a circular ROI by the laser pulse emission. Single dendritic spines of hippocampal neurons were set as ROI and 5 images were acquired with 5 s of intervals as pre-photobleached sampling. Spines were photobleached for 2.5 s with an Argon 488 laser and the recovery of fluorescence was traced for 150 s by acquiring images at 5 s of intervals. The average intensity values of ROI and total image fluorescence were obtained from each FRAP image. Subsequently, the ROI value measured over the time was plotted in the recovery curve. Fluorescence intensities in the bleached spines were normalized to resting values. The continuous lines were given by equation I.

$$\text{Equation I} : F(t) = 1 - f_i - f_m\, e^{(-t/\lambda)}$$

where,

f_i is the fraction of total actin that is stable (immobile)

f_m is the fraction of total actin that turns over rapidly (mobile)

λ is the time constant

Electrophysiology

GFP-positive pyramidal neurons after GFP-tagged shRNA-nArgBP2(pAAV-U6-GFP-shRNA-nArgBP2) or scrambled-shRNA transfection were voltage-clamped to -70 mV or to 0 mV using an Axopatch 200B amplifier and Clampex 10.3 (Molecular Devices, Sunnyvale, CA), filtered at 2k Hz, and sampled at 10k Hz at RT. For rescue experiment, DsRed-tagged shRNA-nArgBP2 was cotransfected with GFP-nArgBP2-res or GFP-⊿SH3-nArgBP2-res. Recording pipettes (2-6 MΩ resistance) were filled with Cesium methanesulfonate(CH_3O_3SCs) internal solution which contained the following: 115 mM CH_3O_3SCs, 20 mM CsCl, 10 mM HEPES, 2.5 mM $MgCl_2$, 0.6 mM EGTA, 4 mM Na_2-ATP, 0.4 mM Na_2-GTP, and 10 mM Na-phosphocreatine. A modified Tyrode's solution used as extracellular solution (150 mM NaCl, 4 mM KCl, 10 mM Glucose, 10 mM HEPES, 2 mM $CaCl_2$ and 2 mM $MgCl_2$, pH 7.4).

To record miniature excitatory postsynaptic currents (mEPSCs), GFP positive neurons were clamped at -70 mV in the presence of picrotoxin (50 μM, Sigma) and tetrodotoxin (TTX, 1 μM). To isolate miniature inhibitory postsynaptic currents (mIPSCs), GFP positive neurons were clamped at 0 mV in the presence of 6-cyano-7-nitroquinoxaline-2,3-dione (CNQX, 10 μM), AP5 (50 μM) and 1 μM TTX. All the antagonists

except picrotoxin were purchased from Tocris Bioscience. The experimenter was blind to the transfected condition of cultures and spontaneous transmission events were analyzed manually to minimize false-positive and false-negative events using MiniAnalysis software (Synaptosoft).

Classification of dendritic spines

To categorize the spines, fluorescent images were imported into NeuronStudio (32), which allows for the automated detection of dendrites and spines. NeuronStudio then measures aspect ratio, head-to-neck ratio, and spine head diameter of individual spines and classify the spine types. These data were then imported into Excel for statistical analysis.

Induction of chemical LTP

AAV-GFP-control or AAV-GFP-shRNA-nArgBP2 transfected neurons (DIV 21-22) were incubated with 50 μM AP5 in neurobasal media. After 48 hr, neurons were transferred to imaging chamber and stimulation solution (200 μM glycine, 20 μM bicuculline, 1 μM strychinine, 0.5 μM TTX in Mg^{2+} free Tyrode) was directly added to induce cLTP and

incubated for 3 min. Then the solution was changed to Tyrode's solution with AP5 and imaged for 30 min with 10 min interval.

3D SIM imaging and data processing

Cultured hippocampal neurons for imaging were prepared as described above. Neurons mounted in a chamber were imaged using N-SIM based on an inverted microscope (ECLIPSE Ti-E, NIKON), equipped with an oil immersion TIRF objective lens (Apo TIRF 100× N.A. 1.49, NIKON), and an EMCCD camera (iXon DU-897, Andor Technology).

All image processing steps were performed in three dimensions. The acquired datasets, comprising 48 axial sections of 512 × 512 pixels, were computationally reconstructed using a reconstruction stack algorithm of NIS-Elements AR (NIKON). The voxel size of the reconstructed images was 32 nm in the x- and y-dimensions and 120 nm in the z-dimension, with 16-bit depth.

Then the reconstructed SIM image stacks were processed by thresholding based on Otsu's method and geodesic active contours to refine the boundaries. Using these two image processing techniques, a custom MATLAB script was developed to handle the SIM image stack (33). The voxel data of resultant binary image stack were converted to

surface mesh data and the polygon meshes of dendritic segments were then loaded into an open-source 3D computer graphics software (Blender, the Blender Foundation) for detection and isolation of polygon meshes for dendritic spines. These spine mesh objects were automatically analyzed by techniques for feature extraction from 3D mesh models or by discrete differential-geometry operators (33).

RESULTS

Domain structure and interactions of nArgBP2

nArgBP2 is a neural variant of ArgBP2 (Arg binding protein 2, also known as SORBS2), first cloned from rat brain as a SAPAP binding protein(2). The full-length protein composed of 1,196 amino acids containing multiple domains for protein-protein interaction including Sorbin Homology (SoHo) domain in the N-terminal region and three Src homology 3 (SH3) domains in the C-terminal region(4). nArgBP2 has one zinc finger motif in the middle region (**Figure 1**).

nArgBP2 is a scaffold protein that controls the balance between adhesion and motility by modulating the function of multiple signaling pathways that converge on the actin cytoskeleton (4). The N-terminal SoHo domain interacts with α2-spectrin and the three SH3 domains have partially overlapping binding partners, with the second SH3 displaying the most numerous interactors including SAPAP(2), synaptojanin1,2(34), vinculin(2), Abl(6), Cbl(5) and dynamin1,2(4). Other interactors are actin regulating Wiskott-Aldrich syndrome protein family verprolin homologous protein (WAVE) 1 and 2, and components of a WAVE regulatory complex (PIR121 and Nap1)(4, 35, 36). ArgBP2 mediates the formation of a complex containing Abl and Cbl, which promotes the Abl-dependent phosphorylation of Cbl and the ubiquitination by Cbl of both

Abl and ArgBP2 (5). In the brain, Abl interacts with Abelson interacting protein-1 (Abi-1) that binds to SHANK and is essential for dendrite morphogenesis and synapse formation (37). nArgBP2 interacts with SHANK either directly or indirectly through SAPAP(2), suggesting the possible network formation among nArgBP2, SAPAP and SHANK.

Localization of nArgBP2 in cultured hippocampal neurons

In cultured hippocampal neurons, nArgBP2 signals were primarily detected in punctate clusters in dendrites that colocalized with the excitatory postsynaptic scaffolding protein PSD95 **(Figure 2A, E)**. Dendritic clusters of nArgBP2 were also juxtaposed with the vesicular glutamate transporter 1 (vGLUT1; an excitatory presynaptic protein) puncta in spiny neurons **(Figure 2B)**. In contrast, nArgBP2 staining rarely overlapped with the inhibitory postsynaptic scaffolding protein gephyrin in spiny neurons **(Figure 2C, E)** and is almost absent in aspiny gephyrin-positive neurons **(Figure 2D)**. Consistently, nArgBP2 clusters hardly colocalized with the vesicular GABA transporter (vGAT; an inhibitory presynaptic protein) puncta in dendrites of pyramidal neurons **(Figure 3A)**. I further found that nArgBP2 clusters were mainly detected in neurons negative for the GABA synthetic enzyme glutamic acid decarboxylase GAD67, while only nuclear and diffuse signals were

observed in GAD67-positive GABAergic neurons (Figure 3B). Thus, I conclude that nArgBP2 primarily localizes to excitatory synapses in spiny pyramidal neurons and plays a specific functional role in these excitatory synapses.

nArgBP2 expression regulates dendritic spine formation

To assess the physiological effects of nArgBP2 on spine formation, I generated small hairpin RNA (shRNA) targeting all isoforms of nArgBP2 in neurons. Suppression of nArgBP2 expression by shRNA was confirmed by Western blot analyses of GFP-nArgBP2 transfected HEK293T cells and cultured cortical neurons (Figure 4A-D). To investigate the effect of nArgBP2 KD on dendritic spine formation, neurons were transfected at 9 *days in vitro* (DIV 9) with shRNA or scrambled shRNA, and were fixed at DIV 16. I found that density of total dendritic protrusions was decreased in nArgBP2 KD, but the most striking effect was on dendritic spine morphology. nArgBP2 KD resulted in a dramatic decrease in the proportion of mushroom-shaped spines (18.83 ± 3.20 for control, 4.16 ± 1.11 for KD, Figure 5A, B) and a concomitant increase in the proportion of long, thin filopodia-like protrusions (Figure 5A, C). When a GFP- full-length nArgBP2 that is resistant to shRNA (GFP-nArgBP2-*res*) was introduced into KD neurons, the defect on dendritic spine morphology was fully rescued,

ruling out any off-target consequence of shRNA-nArgBP2 expression (**Figure 5D-F**). The SH3 domain-deletion mutant (GFP-⊿SH3-nArgBP2-*res*), however, failed to rescue KD phenotype, indicating that the interaction via its SH3 domains is required (**Figure 5D-F**).

nArgBP2 KD selectively impairs excitatory spine-synapse formation

Dendritic spines are actin-rich architectures that receive presynaptic inputs in most excitatory synapses of the central nervous system (38). The aberrant spine morphology caused by nArgBP2 KD implies possible defects in spine-bearing synapses. To monitor excitatory/inhibitory synaptogenesis *in vitro*, neurons were cultured at low density and were labeled with antibodies against presynaptic vGLUT1 and postsynaptic PSD95 or presynaptic vGAT and postsynaptic gephyrin to distinguish between putative excitatory and inhibitory synapses, respectively (**Figure 6A-D**). Presynaptic development was similar in both neurons as assayed by quantification of vGLUT1 or vGAT-positive puncta (puncta per 50 μm of dendrite length, vGLUT1: 19.04 ± 1.13 for control, 17.31 ± 1.81 for KD; vGAT: 17.49 ± 1.14 for control, 17.80 ± 1.72 for KD), demonstrating that nArgBP2 KD did not interfere with the establishment of presynaptic contacts. Intriguingly, I observed that excitatory contacts between vGLUT1 and PSD95 in KD predominantly formed at dendritic

shafts instead of a juxta-dendritic position typical for contacts on spine heads in spiny neurons (Figure 6A, B). The number of synapse on spines was decreased dramatically with concomitant increase of synapse on shafts (18.20 ± 2.50 on spines, 1.91 ± 1.08 on shaft for control, 1.90 ± 0.83 on spines, 15.81 ± 2.50 on shaft for KD, Figure 6B). The location of vGAT-gephyrin-positive inhibitory contacts on dendritic shafts appeared unchanged (Figure 6A, B). In contrast, excitatory and inhibitory synapses in aspiny neurons were not altered by KD (Figure 6C, D). These data indicate that nArgBP2 KD causes a specific reduction of spine-bearing synapses, which is also consistent with the above observed decrease in matured mushroom-shaped spines in nArgBP2 KD neurons.

nArgBP2 KD reduces the mean frequency of miniature excitatory postsynaptic currents

I next evaluated the functional consequence of nArgBP2 KD on synaptic transmission. nArgBP2 KD significantly reduced the mean frequency of miniature excitatory postsynaptic currents (mEPSCs) whereas the amplitude of the mEPSCs was unaffected (Figure 7A, B). nArgBP2 KD had no effect on miniature inhibitory postsynaptic currents (mIPSCs) in both frequency and amplitude (Figure 7C, D), again supporting its selective role in controlling spine-bearing excitatory synapses. I further

showed that GFP-nArgBP2-*res,* but not GFP-⊿SH3 nArgBP2-*res,* rescued the defects in mEPSC frequency by KD, indicating the involvement of SH3 domain-mediated interactions (**Figure 7E, F**).

nArgBP2 KD increases WAVE / PAK / cofilin phosphorylation

To address the possible molecular mechanisms linking the loss of nArgBP2 to aberrant spine morphology, I studied actin cytoskeleton modifications. F-actin is a major component of both dendritic spines and filopodia that is dramatically remodeled during synaptic contact formation and stabilization (39-41). It was previously found that nArgBP2 interacts with multiple proteins working primarily on the regulation of the actin cytoskeleton such as WAVE and proteins of the WAVE regulatory complex like PIR121 and Nap1 (4). Thus, I followed the state of activation of WAVE in nArgBP2 KD cortical neurons. Accordingly, I found an increased level of phosphorylated-WAVE1 (**Figure 8A**), the active form of the protein in neurons expressing shRNA-nArgBP2.

WAVE is activated by Rac1, a member of the Rho family of small GTPases, which also promotes phosphorylation/inactivation of the actin depolymerizing factor cofilin via PAK-LIMK cascade (13, 42). Since the role of PAK and cofilin on dendritic spine morphogenesis is well

established (16, 43-45), I hypothesized that loss of nArgBP2 may enhance Rac1 activity leading to activation of PAK and subsequent inactivation of cofilin, which ultimately may cause the loss of mature mushroom-type spines and the overabundance of immature filopodia-like protrusions. Indeed, I observed an upregulation of phosphorylation of both PAK and cofilin in nArgBP2 KD (**Figure 8B, C**), indicating that nArgBP2 KD causes activation of WAVE1 and PAK, and a subsequent inactivation of cofilin (**Figure 8D**). Furthermore, I found that the inhibition of PAK by coexpression of a PAK-inhibitory domain (PID) or the coexpression of a constitutively active cofilin mutant S3A both partially rescued the dendritic spine phenotype caused by nArgBP2 KD (**Figure 10A-E**).

Because nArgBP2 KD activates both WAVE and PAK pathways, by just inhibiting PAK may not be enough to rescue the phenotype fully. To prove this hypothesis, I decided to block both WAVE and PAK activity in nArgBP2 KD background. Previously it was found that among three SH3 domains of nArgBP2, the first and the second bind to WAVE, whereas the third does not(4). Thus, I used mitochondria-targeting SH3-1/2 and SH3-3 domains (mSH3-1/2 and mSH3-3). As expected, mSH3-1/2 (but not mSH3-3) sequesters WAVE from the cytosol to the mitochondria (**Figure 9**). Using these tools, I showed that the sequestration of WAVE by mSH3-1/2 partially rescues the dendritic

spine phenotype caused by nArgBP2 KD (**Figure 11**).

Furthermore, I found that the inhibition of PAK by PID, or cofilin by S3A, combined to sequestration of WAVE by mSH3-1/2 almost totally rescue the aberrant spine phenotype caused by nArgBP2 KD (**Figure 10A-E**). Together, these results strongly indicate a causal relation between elevated WAVE/PAK/cofilin phosphorylation and the aberrant dendritic spine morphology observed in nArgBP2 KD neurons.

nArgBP2 KD causes a marked increase of actin cytoskeleton dynamics in spines

Previous study demonstrated that the ArgBP2/nArgBP2 KD in astrocytes causes major changes in actin dynamics (4). I used live-cell imaging techniques to follow the spatial-temporal dynamics of actin in dendritic spines. I derived outline profiles of individual spines in successive frames and used to calculate a shape factor.

Changes in spine morphology were assessed using the 'shape factor' routine ($sf = 4\pi A/p^2$) in the Metamorph program, which is calculated from the perimeter p and the area A of the object (46). The circularity value approaches 1 as the spine head is rounder and closer to 0 as the spine head is more irregular or elongated (**Figure 12A**). The shape factor was used to generate a graphical display of changes in morphology over time and fluctuations in shape factor values provide a

quantitative measure of spine motility. Consequently, I found that the shape factor value oscillates closer to 0.9 in control neurons (**Figure 12B**), indicating that spine morphology is stable and the shape is rounder in these cells. In nArgBP2 KD spines, however, wider fluctuations in the shape factor spanning from 0.4 to ~ 0.8 were observed, suggesting the irregular shapes of KD spines and the highly dynamic nature of actin cytoskeleton in these spines (**Figure 12C**).

To further study the intracellular dynamics of actin within spines, I performed fluorescence recovery after photobleaching (FRAP) experiments in neurons expressing GFP-tagged actin. Individual spines were photobleached and the time course of the subsequent fluorescence recovery was used as an indicator of actin dynamics (**Figure 13A**). Since actin filaments within the spines are in the filamentous form and actin filaments within are in a dynamic equilibrium, new fluorescent monomers will be continuously incorporated into filaments, replacing the bleached ones. Therefore, the recovery of fluorescence reflects the rate of turnover of actin.

In control spines, the average time constant for recovery of GFP-actin after photobleaching was 29.99 ± 1.65 s; 80.3 ± 1.14 % of total actin was in a dynamic state, and 19.7 ± 1.09 % was stable (**Figure. 13B-D and Table 1**). In nArgBP2 KD, the rate of turnover of actin was not significantly altered (time constant 28.12 ± 1.40 s), but almost all of actin (95.1 ± 1.16 %) was in a dynamic state, whereas only 4.90 ±

0.54 % of the total was stable (**Figure. 13B-D and Table 1**). Finally, treatment of neurons with 10 μM N^6-[2-[[4-(diethylamino)-1-methylbutyl] amino]-6-methyl-4-pyrimidinyl]-2-methyl-4,6-quinolinediamine trihydrochloride (NSC23766), a selective inhibitor of Rac1-GEF, completely abrogated the effect of nArgBP2 KD on actin composition, again indicating that Rac1 activation is a downstream effector of nArgBP2 KD (**Figure. 13B-D and Table 1**).

The experimental results so far indicate that that nArgBP2 functions to regulate spine morphogenesis and subsequent spine-synapse formation at glutamatergic synapses and that its ablation causes a robust and selective inhibition of excitatory synapse formation by altering actin cytoskeleton dynamics (**Figure 14**).

nArgBP2 KD does not cause morphological change in mature neuron

nArgBP2 seems to work for well-designed structural construction of dendritic spines and an apparent defect of nArgBP2 KD has been observed in the developing neurons (DIV 14 to 16). I concluded that nArgBP2 may be needed when significant structural remodeling is required. To study the nArgBP2 KD effect at the mature stage, shRNA was transfected at DIV 15-16 and observed at DIV 21-22 when structurally robust dendrites were already formed. Unlike the dramatic

morphological changes observed in the KD group in developing neurons, both the control and shRNA groups of mature neurons showed very similar phenotypes (Figure 15A). According to quantification analysis using NeuronStudio (32), the ratio of mushroom, stubby and thin spines was similar in both control and shRNA group (Figure 15B). The distinct effect of nArgBP2 KD, which was observed only at the development stage but not at the mature stage, again supports the hypothesis that it plays an important role in the formation of dendritic spines which requires active actin cytoskeleton construction.

nArgBP2 KD causes impairment of spine enlargement under cLTP condition in mature neuron

Dendritic spines actively participate in the formation of synapses and neuronal circuits during development(47) whereas activity-dependent spine maintenance or elimination is important for the remodeling of established neuronal circuits during post-natal and adolescence periods (48, 49). Persistent changes of synaptic strength during synaptic plasticity also involve structural changes of spines.

To further examine the role of nArgBP2 in regulation of spine morphology at mature stage, I carried out time-lapse live-cell imaging. For these experiments, I used GFP as the morphological marker. To induce the structural fluctuation of dendritic spine, I used the synaptic

plasticity paradigm of chemically-induced long-term potentiation (LTP), which involves raising neuronal activity by briefly incubating with a modified Tyrode's solution that globally potentiates synapses. cLTP, which induces new synapse formation in mature neurons, causes structural plasticity to change the size of the dendritic spine, which generally increases in size.

I first performed time-lapse imaging of the same set of dendritic spines in cultured hippocampal neurons at 0, 10, 20 and 30 min after induction of cLTP (**Figure 16A and B**). In control neurons, relative size of dendritic spines gradually increased over 30 min after induction of cLTP whereas those in shRNA neurons slightly decreased(3.19 ± 0.73 for control, 0.77 ± 0.12 for shRNA, **Figure 16B**). This provided a clue that nArgBP2 KD caused loss of control of the actin dynamics required for actin cytoskeleton remodeling. This also suggests that nArgBP2 functions not only in structural regulation but also in synaptic plasticity.

Then I used 3D-SIM imaging to detect sophisticated changes in high resolution and to observe fine structural changes of dendritic spines (**Figure 17**). In the same condition with the previous experiment, I acquired 3D-stack SIM image at time point 0 and 30 min. The datasets were reconstructed using NIS-Elements AR (**Figure 17A**) and binarized with a custom MATLAB code(33) (**Figure 17B**). The voxel data of generated binary image stack were converted to surface mesh data and the polygon meshes of dendritic segments were loaded into an open

source 3D graphics software (Blender(50)) for detection and isolation of polygonal meshes of dendritic spines (**Figure 17C, D**).

The polygon meshes of dendritic segments were isolated to individual dendritic spines and analyzed with a custom MATLAB code to measure the 3D geometry-based morphological features. The features include surface area (S), volume (V), length (L), maximum head diameter (hMax), maximum neck diameter (nMax), and head to neck ratio (HNR) (**Figure 18A**). The hMax, nMax, and HNR are the 3D extensions of the 2D image-based feature analysis introduced by Qiao et al. (51). I determined hMax in the local plane with the largest maximum diameter of the spine head part and nMax with the smallest maximum diameter of the neck part. HNR is the ratio of head to neck, which is obtained by hMax/ nMax. S, V, and L represent the morphology of 3D meshes generated, while hMax, nMax and HNR represent the 2D-based features such as head and neck.

I then measured the change in values of values after cLTP normalized to initial values (Δchange, **Figure 18B**). The relative surface area after induction of cLTP increased significantly in the control neurons slightly decreased in the shRNA neurons (S; 0.56 ± 0.12 for control, −0.055 ± 0.06 for shRNA, **Figure 18B**). The volume has doubled in control neurons but remained almost the same in the shRNA neurons (V; 1.26 ± 0.32 for control, 0.04 ± 0.09 for shRNA, **Figure 18B**). The length of spine has

slightly increased in control while decreased in shRNA (L; 0.13 ± 0.06 for control, −0.13 ± 0.05, 0.86 ± 0.05 in shRNA, Figure 18B). The three features of 3D mesh data represent different trends but share significant differences between control and nArgBP2 KD neurons. 2D-based features, relative hMax, nMax and HNR also showed significant difference as in previous experimental results (hMax; 0.46 ± 0.11 for control, 0.06 ± 0.06 for shRNA, nMax; 0.34 ± 0.09 for control, 0.46 ± 0.09 for shRNA, HNR; 0.23 ± 0.10 for control, −0.14 ± 0.10 for shRNA, Figure 18B).

These experiments demonstrate a crucial role for nArgBP2 in mediating LTP-induced spine enlargement via its interaction with the actin cytoskeleton quite probably involving WAVE/PAK/cofilin pathway. The results also imply that nArgBP2 functions not only in structural regulation in developing neurons but also in synaptic plasticity which involves active remodeling of actin cytoskeleton in dendritic spines.

FIGURES

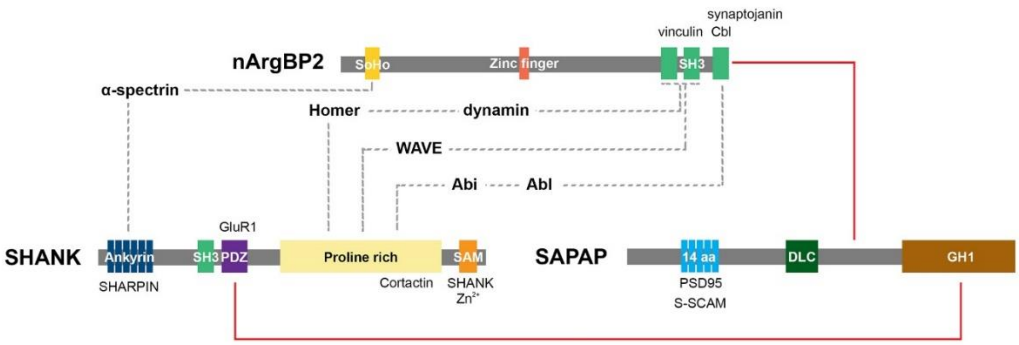

Figure 1 The domain architectures and protein interaction of nArgBP2.

Proteins listed with each of the domain indicate the known binding partners. Only a subset of known interacting proteins is shown. nArgBP2, SHANK and SAPAP interact with each other either directly via specific domains (red lines) or indirectly through the common binding partners (broken lines). SAPAP interacts with nArgBP2 via its proline rich region between DLC and GH1 regions. Abbreviations: **14 aa**, 14 amino acids domain; **Abi**, Abelson interacting protein-1; **DLC**, dynein light chain; **GH1**, GKAP homology 1; **nArgBP2**, neural Arg binding protein 2; **PDZ**, PSD95, Dlg1, and zo-1; **PSD95**, postsynaptic density protein 95; **SAM**, Sterile alpha motif; **SAPAP**, SAP90/PSD95-associated protein; **SHANK**, SH3 and multiple ankyrin repeat domains; **SH3**, Src homology 3 domain; **SoHo**, Sorbin homology domain; **S-SCAM**, synaptic scaffolding molecule; **WAVE**, WASP (Wiskott-Aldrich syndrome protein)-family verprolin homologous protein.

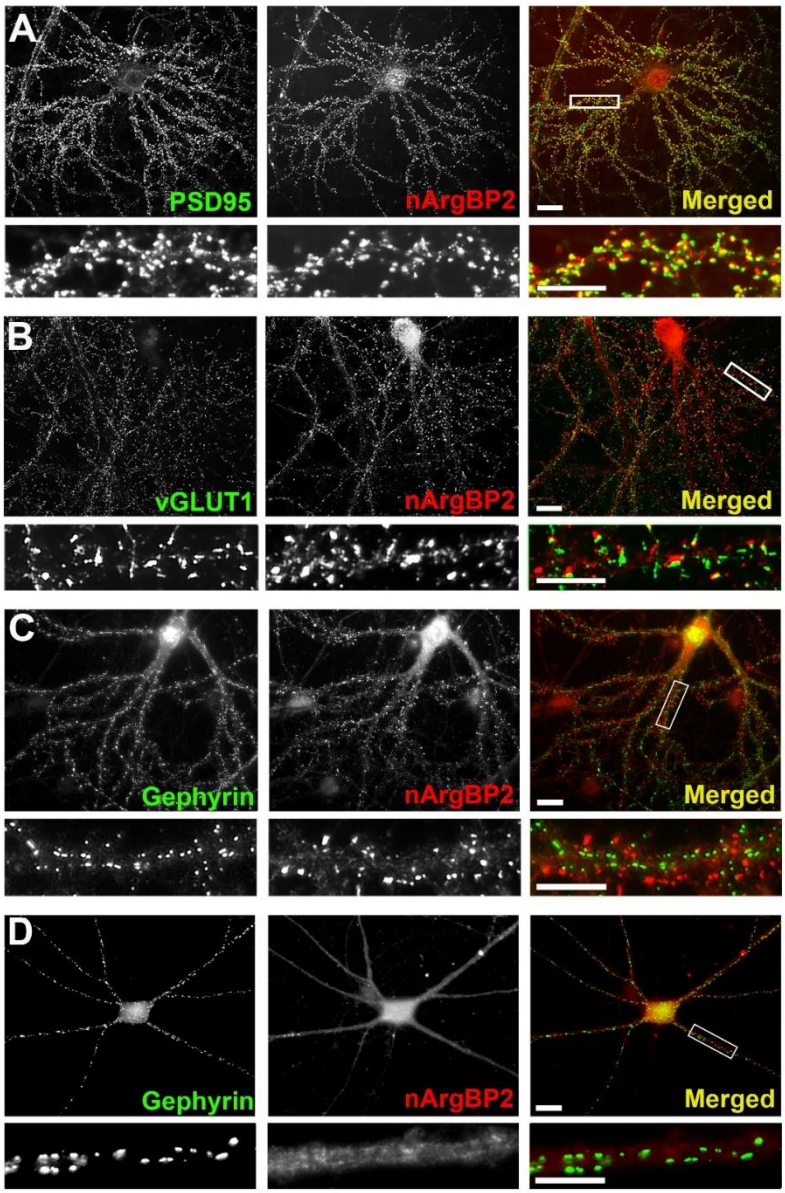
A
PSD95
nArgBP2
Merged
B
vGLUT1
nArgBP2
Merged
C
Gephyrin
nArgBP2
Merged
D
Gephyrin
nArgBP2
Merged
E
*
MCC (M1 & M2)
1
0.8
0.6
0.4
0.2
0
PSD95
Gephyrin

Figure 2 nArgBP2 primarily localizes to excitatory synapses in spiny neurons.

A, B, nArgBP2 clusters colocalized with PSD95 (**A**) and also were found to be juxtaposed with the vesicular glutamate transporter 1 (vGLUT1) puncta in pyramidal spiny neurons (**B**). The bottom images are enlarged views of the boxed regions. **C, D,** nArgBP2 clusters did not colocalized with gephyrin in spiny neurons (**C**) and were almost absence in aspiny neurons (**D**). **E**, Manders' colocalization coefficients (MCCs) of nArgBP2 clusters with PSD95 or gephyrin signals in dendritic regions of hippocampal neurons. M1 (yellow bars) indicates the fraction of nArgBP2 overlapping PSD95 or gephyrin and M2 (green bars) indicates the fraction of PSD95 or gephyrin overlapping nArgBP2 (M1: 0.78 ± 0.02 for PSD95, 0.08 ± 0.02 for gephyrin; M2: 0.85 ± 0.01 for PSD95, 0.08 ± 0.01 for gephyrin). Scale bars: 20 μm; 10 μm; (enlarged)

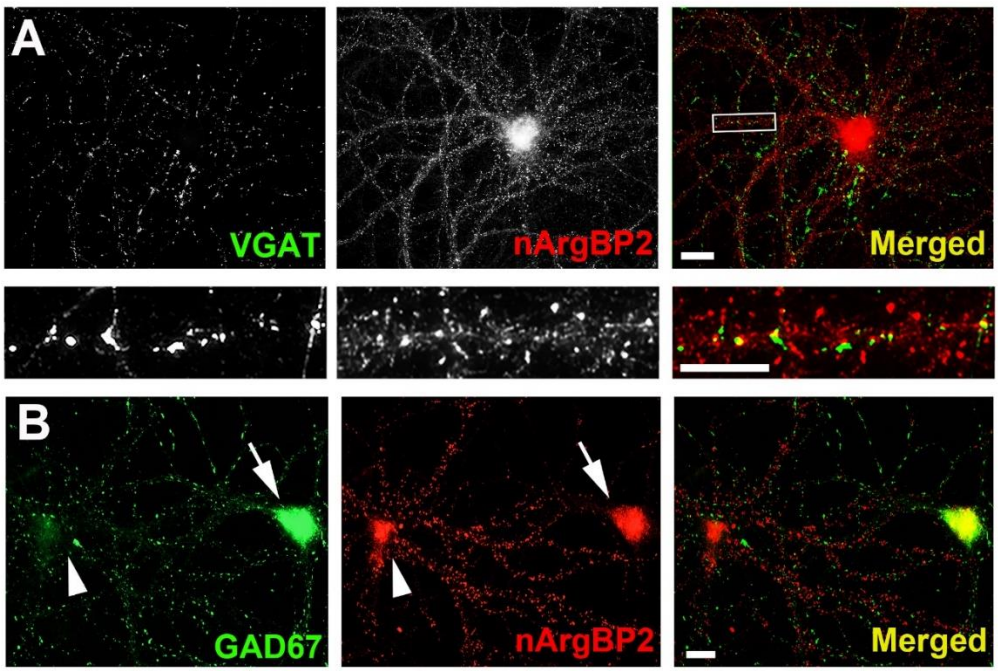

Figure 3 nArgBP2 rarely localizes to inhibitory synapses in neurons.

A, Cultured hippocampal neurons at DIV 21 were doubly labeled for nArgBP2 and GAD67 (A) or vGAT (B). nArgBP2 rarely colocalized with vGAT in spiny neurons. The bottom images are enlarged views of the boxed regions. B, Arrowhead and arrow indicate cell bodies of GAD67−negative neurons and GAD67−positive neurons, respectively. Scale bars: 20 μm; 10 μm; (enlarged).

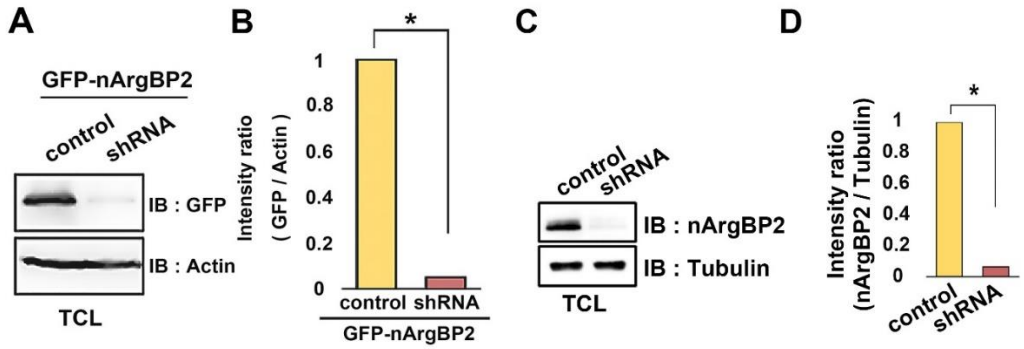

Figure 4 shRNA-mediated KD efficiency confirmed by Western blot analysis.

A, B, HEK293T cells were co-transfected with GFP-nArgBP2 and shRNA-nArgBP2. The knockdown efficiency was analyzed by Western blotting 72 h after transfection with anti-GFP antibody. *$p < 0.05$; Student's t test. C, D, Cortical neurons at DIV 6 were infected with adeno-associated virus (AAV)-shRNA-nArgBP2 and the knockdown efficiency was confirmed by Western blotting with anti-nArgBP2 antibody at DIV 21.

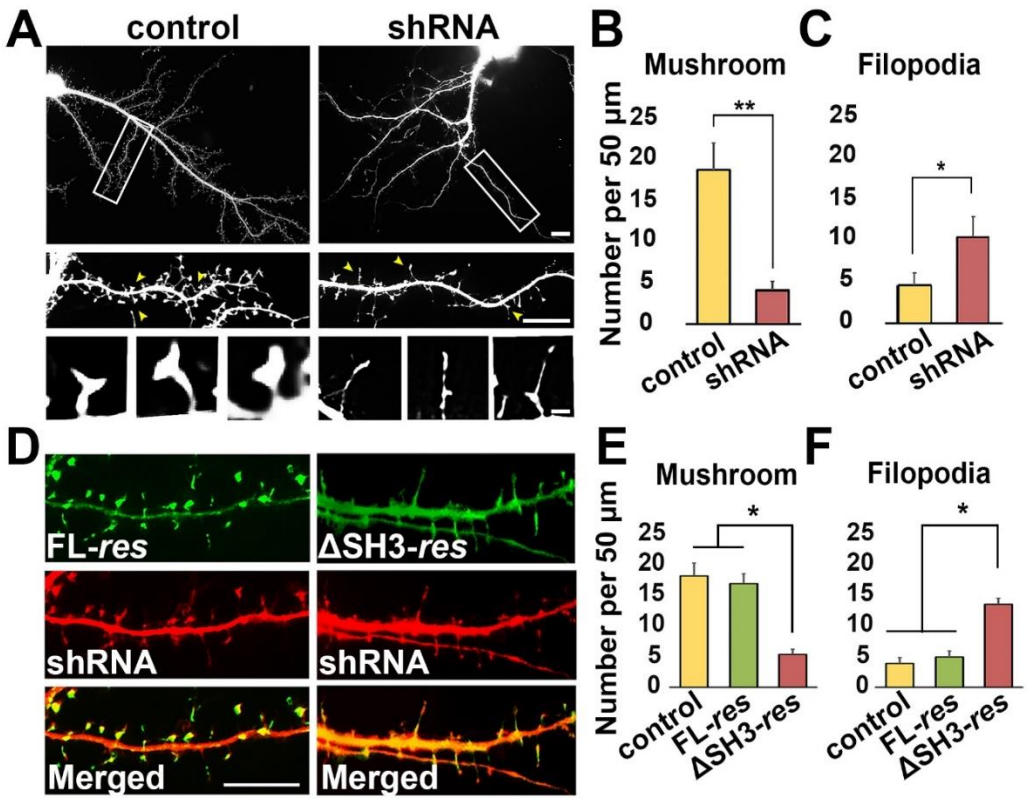

Figure 5 Knockdown of nArgBP2 decreases mushroom-shaped spines and increases in the filopodia-like protrusions.

A, Representative spine morphologies from dendrites of neurons expressing scrambled (control) or shRNA-nArgBP2. Neurons were transfected at DIV 9 and fixed at DIV 16. Lower panels are enlarged images of parts enclosed with rectangles. Three representative examples of mushroom spines from control neurons, and the same number of filopodia-shaped protrusions from nArgBP2 KD are shown at the bottom panels. Scale bars; 20, 20 and 2 μm respectively. B, C, The number of

mushroom-shaped spines (**B**) and filopodia (**C**) from control and shRNA-transfected neurons. *p < 0.05, **p < 0.01 Student's *t*-test, n = 54 neurons from 6 independent cultures. **D,** Representative images of spine morphologies from dendrites of neurons coexpressing the shRNA with GFP-nArgBP2- or GFP-⊿SH3-nArgBP2 resistant constructs. *res* indicates the presence of a silent mutation that is resistant to shRNA. Scale bars; 20 μm. **E, F,** The number of mushroom-shape spines (**E**) and filopodia (**F**). n = 36 neurons from 5 independent cultures.

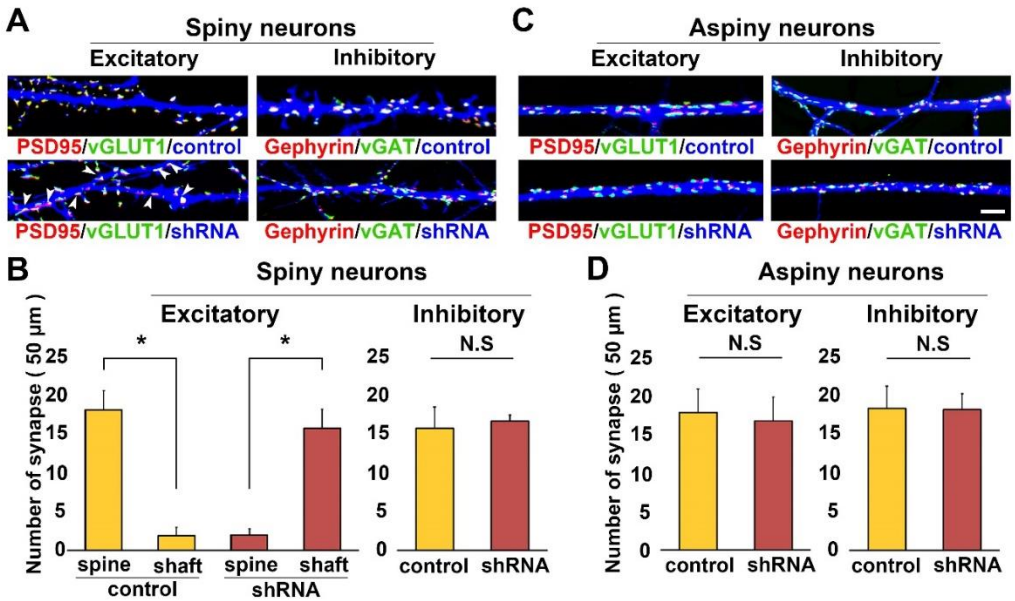

Figure 6 nArgBP2 KD impairs excitatory spine-synapse formation while does not affect inhibitory synapses.

A, B, Immunocytochemistry of dendrites from scrambled (control) and nArgBP2 KD (shRNA) spiny neurons (DIV 21) co-labeled with antibodies against vGLUT1 and PSD95 or vGAT and gephyrin to visualize pre- and postsynaptic elements of excitatory or inhibitory synapses, respectively. Arrowheads point to PSD95 clusters that form at dendritic shafts instead of dendritic spines. C, D, Analogous experiments to reveal excitatory and inhibitory synaptic contacts in aspiny neurons. The original color for gephyrin was blue by the Alexa-405 secondary antibody, but in order to generate a more contrasted picture, I pseudo-colored gephyrin signal to red and to blue the DsRed expressed by the

shRNA vector. The number of excitatory synaptic contacts on dendritic spines in spiny neurons (identified by the juxtaposed localization of vGLUT1 and PSD95 puncta) was dramatically reduced in KD neurons, while the number of inhibitory synaptic contacts on dendritic shaft (identified by the juxtaposed localization of vGAT and gephyrin signals) was not changed. Neither excitatory nor inhibitory contacts in aspiny neurons were altered. All data are means ± s.e.m. $*p < 0.01$, n = 52 neurons from 5 independent cultures. N.S.: not significant. Scale bars; 5 μm.

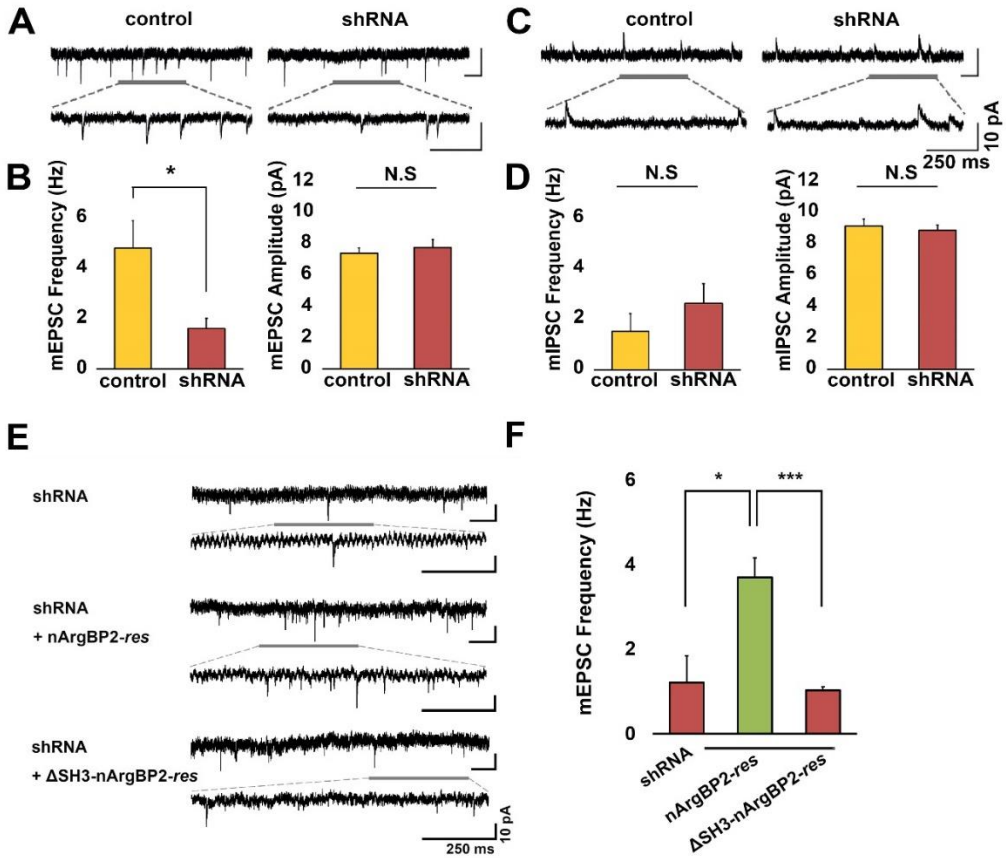

Figure 7 nArgBP2 KD alters the mean frequency of miniature excitatory postsynaptic currents.

A, B, nArgBP2 KD reduced the frequency but not amplitude of mEPSCs. Neurons were transfected at DIV 9 and analyzed at DIV 16. Sample traces of mEPSCs are shown in A. n = 9 for control (scrambled) and for KD. C, D, nArgBP2 KD had no effect on the frequency or amplitude of mIPSCs. n = 7 for control and 8 for KD. Sample traces of mIPSCs are shown in C. E, F, Cultured hippocampal neurons (DIV 9) were transfected with the

shRNA−nArgBP2 construct on its own, which expresses DsRed, or combined to GFP−nArgBP2−*res* or GFP−⊿SH3−nArgBP2−*res,* and were used for recording at DIV 16. Reduction of mEPSC frequency by nArgBP2 KD was rescued by the coexpression with GFP−nArgBP2−*res,* but unaffected by the expression of GFP−⊿SH3−nArgBP2−*res*. Sample traces of mEPSCs are shown in E. $n = 5$ for each group; *, $p < 0.05$. ***, $p<0.001$; Student's *t* test. Error bars indicate mean ± s.e.m.

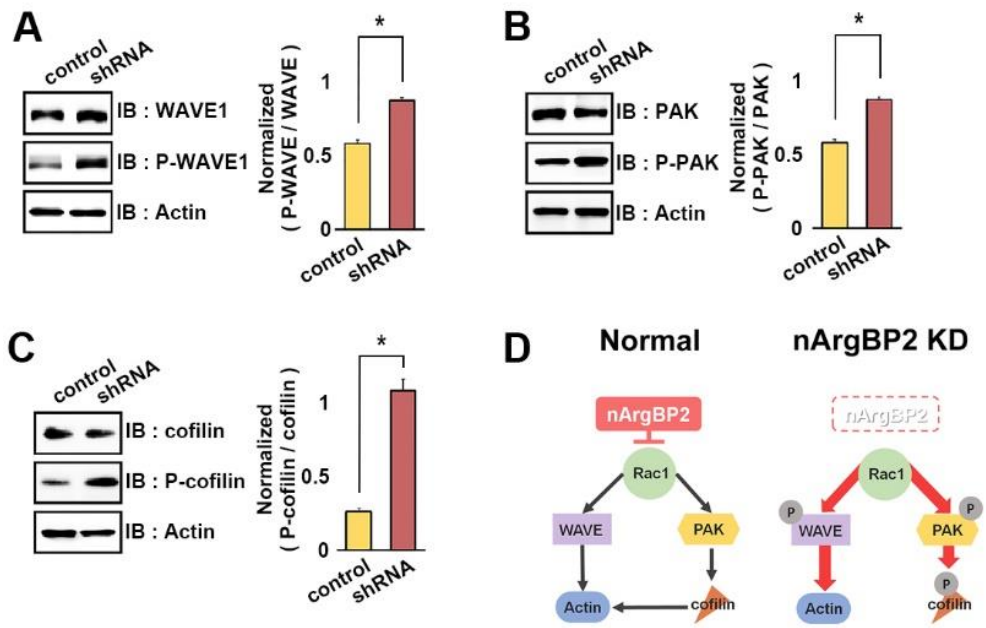

Figure 8 nArgBP2 KD increases WAVE1/PAK/cofilin phosphorylation.

A–C, Cortical neurons infected with AAV–scrambled or shRNA–nArgBP2 at DIV 6 were lysed at DIV 21 and cell extracts were immunoblotted with: anti–WAVE–1 and phospho–WAVE1 antibody. (A); PAK and phospho–PAK antibody (B); and anti–cofilin and (C); phospho–cofilin antibody. n=3 for each group; $*p < 0.05$; Student's *t* test. Error bars indicate mean ± s.e.m. D, Schematic models of nArgBP2 signaling pathways for regulating actin cytoskeleton. In normal condition, nArgBP2 controls actin cytoskeleton dynamics through WAVE and PAK/cofilin cascade. The WAVE/PAK/cofilin phosphorylation are increased in

nArgBP2 KD neurons, indicating that nArgBP2 KD causes activation of WAVE and PAK, and a subsequent inactivation of cofilin.

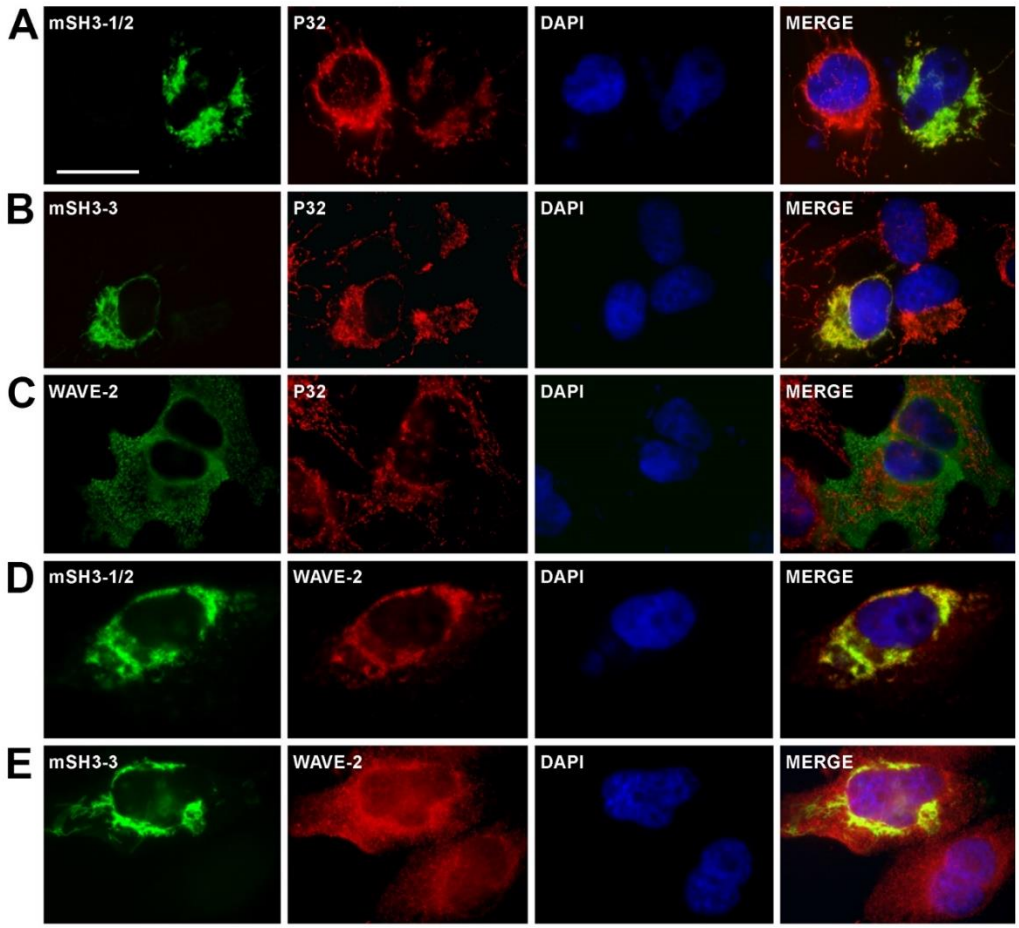

Figure 9 Immunofluorescence staining of cells expressing nArgBP2 SH3 domains and WAVE-2.

A, B, Effect of nArgBP2 SH3 domains on the localization of Flag-WAVE-2. HeLa Cells expressing either GFP-tagged mSH3-1/2 or mSH3-3 of nArgBP2 were labeled with anti-GFP antibodies and with antibodies directed against the mitochondria protein p32. C, HeLa Cells expressing Flag-WAVE-2 were labeled with anti-Flag antibodies and anti-p32. D,

E, HeLa Cells expressing either mSH3-1/2 or mSH3-3 together with Flag-WAVE-2 were labeled by immunofluorescence with anti-GFP and anti-Flag antibodies. mSH3-1/2 or mSH3-3 alone shows a prominent localization on mitochondria, while Flag-WAVE-2 on its own localizes in the cytoplasm. When Flag-WAVE-2 is coexpressed with mSH3-1/2, it is significantly sequestered on the mitochondria, while it remains in the cytoplasm of cells expressing mSH3-3. Scale bar: 10 μm

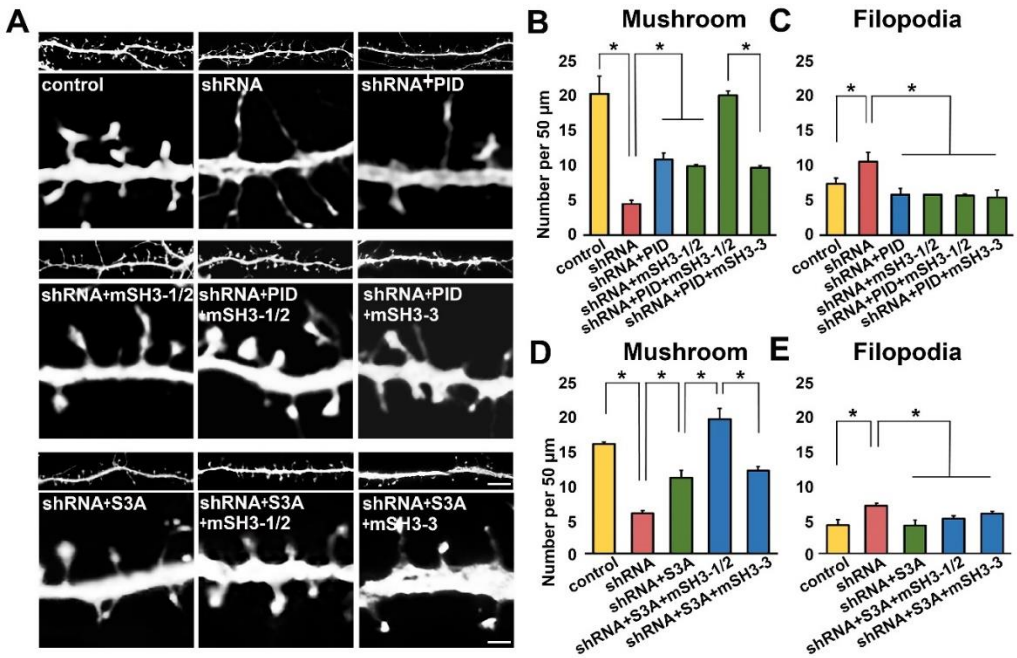

Figure 10 Counteracting WAVE1/PAK/cofilin phosphorylation cascade rescues nArgBP2 KD effects on spines.

A, Representative images of spine from dendrites of neurons expressing each set of constructs. Neurons were transfected at DIV 9 and fixed at DIV 16. Control: scrambled; shRNA: shRNA−nArgBP2; PID: PAK inhibitory domain; S3A: phospho−deficient mutant of cofilin; mSH3−1/2: first and second SH3 domains of nArgBP2 targeted to mitochondria; mSH3−3: the third SH3 domain of nArgBP2 targeted mitochondria. Lower panels are enlarged images of the insets enclosed with rectangles. Scale bars; 10 and 2 μm, respectively. B−E, The number of mushroom−shaped spines (B, D) and filopodia (C, E) from each experimental group *$p < 0.05$; ANOVA followed by Tukey's HSD post hoc test; n = 45

neurons from 7 independent cultures (B, C). n = 39 neurons from 4 independent cultures (D, E).

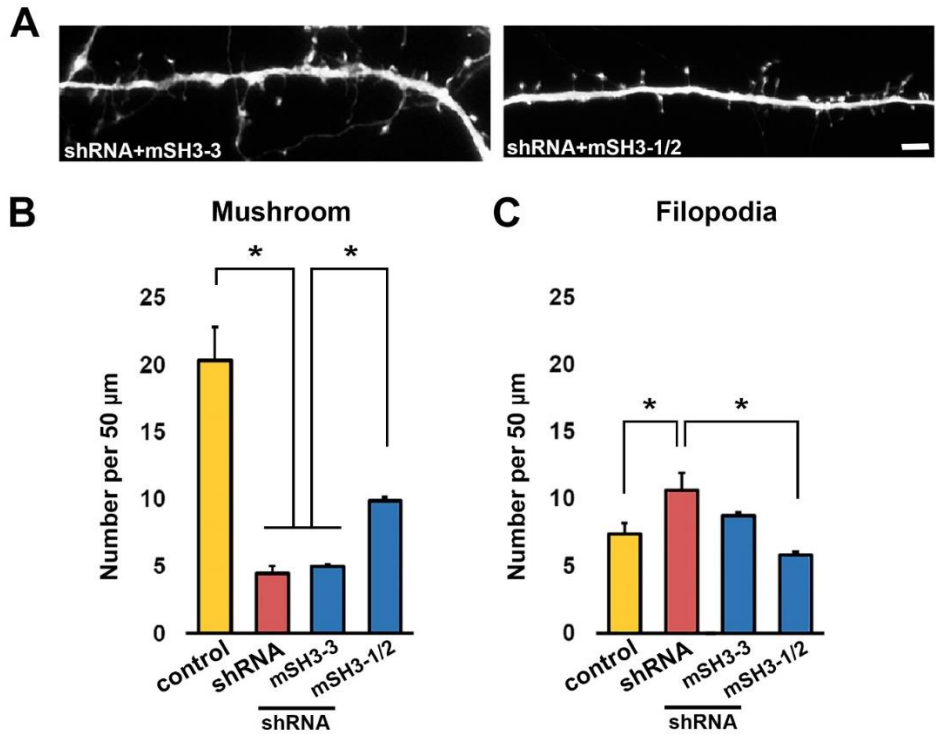

Figure 11 Sequestration of WAVE by mSH3−1/2 partially rescue the aberrant spine phenotype caused by nArgBP2 KD.

A, Representative images of spines from neurons expressing shRNA−nArgBP2 alone, with mSH3−1/2 (first and second SH3 domains of nArgBP2 tagged with GFP and targeted to mitochondria) or mSH3−3 (third SH3 domain of nArgBP2 tagged with GFP and targeted to mitochondria)). Neurons were transfected at DIV 9 and fixed at DIV 16. Scale bars; 5 μm. B, C, The number of mushroom−shaped spines (B) and filopodia (C) from each experimental group $*p < 0.05$; ANOVA followed by Tukey's HSD post hoc test; n = 40 neurons from 9 independent cultures.

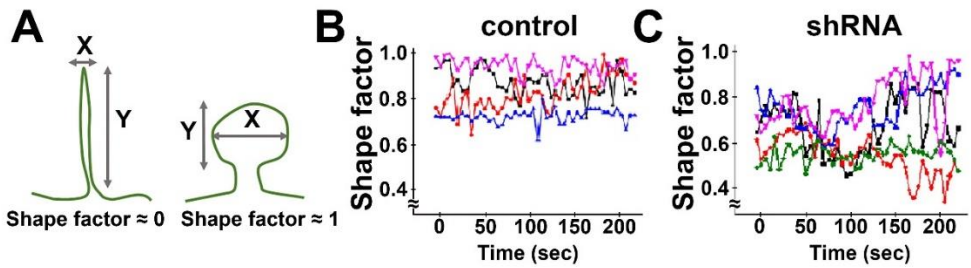

Figure 12 nArgBP2 KD causes a marked increase of actin cytoskeleton dynamics in spines.

A, Shape factor of dendritic spines calculated from time-lapse recordings of actin dynamics following GFP-actin. Changes in spine shape were assessed using the 'shape factor' routine ($sf = 4\pi A/p^2$) of the MetaMorph program, which is calculated from the perimeter p and the area A of each spine head. Values close to 0 represent elongated or ruffled shapes, whereas values around 1 describe a perfect circle. Fluctuations in shape factor values reflect spine motility. B, C, Representative shape factor profiles of control (B) and nArgBP2 KD (C) spines over time. Each color indicates an individual spine. Neurons were transfected at DIV 9 and analyzed at DIV 16. Compared to control, nArgBP2 KD produces irregular or elongated spine shape and a wider fluctuation of the shape factor that indicates rapider spine motility.

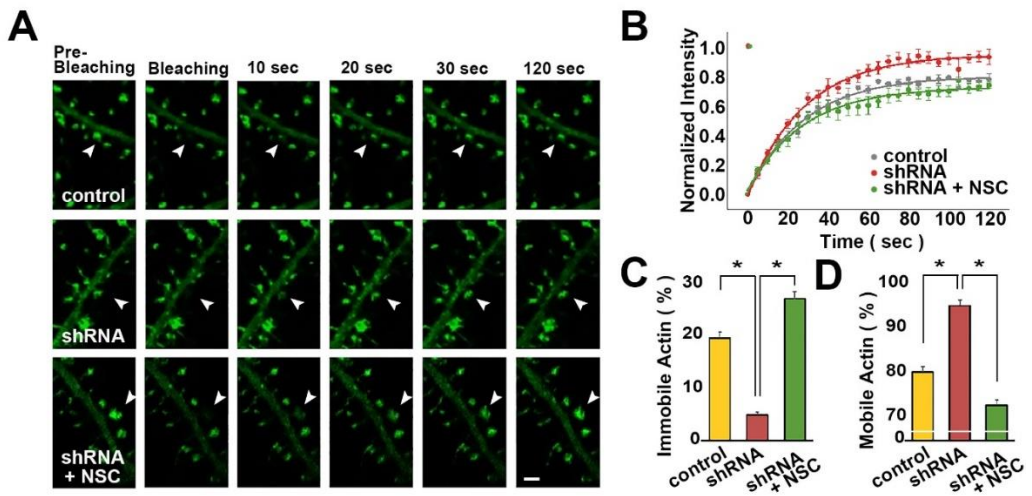

Figure 13 Increased actin cytoskeleton dynamics in nArgBP2 KD neurons is abrogated by Rac1 inhibition.

A, Example of fluorescence recovery in spines after photobleaching. Neurons were transfected with GFP-actin at DIV 9 and studied at DIV 16. The images immediately after photobleaching indicate a complete loss of fluorescence in the bleached spines (arrowheads) while neighboring spines are unaltered. Subsequent time-lapse images show gradual recovery of fluorescence. Scale bars; 2 μm. B, Fluorescence intensity in the bleached spines, normalized to resting values. The continuous lines were given by equation I (Material and Methods). Fluorescence recovery was up to ~80 % of the prebleached levels in control neurons, while it reached up to ~98 % of the prebleached levels in nArgBP2 KD cells. Treatment of neurons with 10 μM of Rac1 inhibitor NSC 23766 completely abrogates the effect of nArgBP2 KD on actin dynamics. C, D,

The proportion of immobile actin (C) and mobile actin (D) in control, nArgBP2KD, and nArgBP2 KD spines treated with NSC 23766 (See Table 1 for exact numbers). *$p < 0.05$; ANOVA followed by Tukey's HSD post hoc test; n = 15 neurons from 5 independent cultures.

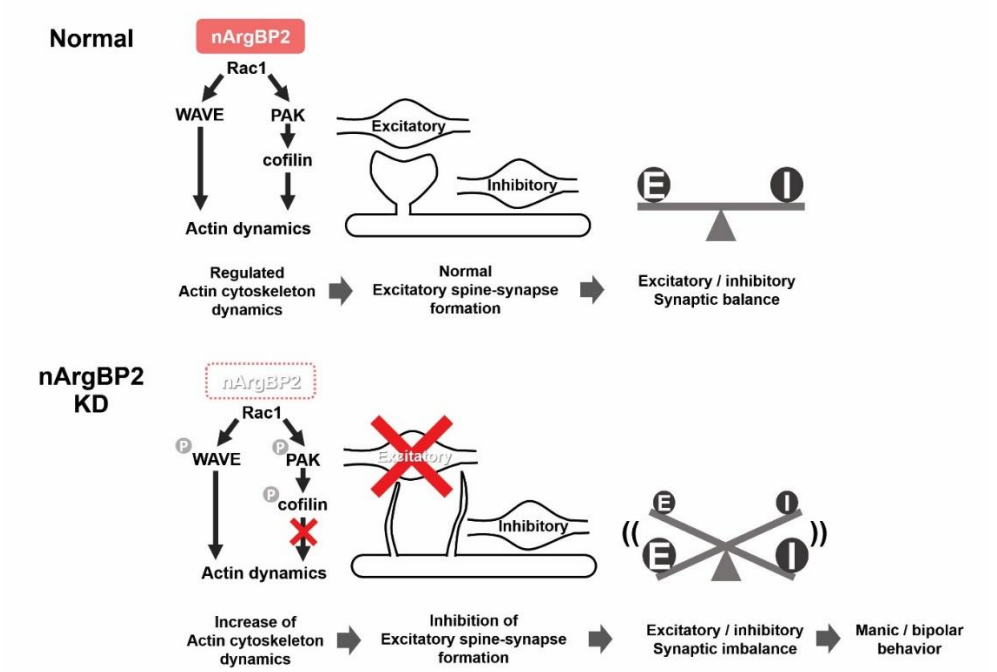

Figure 14 Schematic description of the role of nArgBP2 in excitatory spine-synapse formation and maintenance of E/I balance.

In the normal condition, nArgBP2 plays a role in controlling actin cytoskeleton dynamics through the WAVE and PAK/cofilin cascade. Its ablation, however, increases actin dynamics via uncontrolled phosphorylation of the WAVE/PAK/cofilin pathway, causing a robust and selective inhibition of excitatory spine-synapse formation. This subsequently leads to an excitatory/inhibitory synaptic imbalance. Since the excitatory/inhibitory synaptic imbalance likely leads to a broad spectrum of psychiatric disorders, nArgBP2 KD, which selectively alters excitatory synapse formation, may account for the ID and manic/bipolar-like behaviors observed in nArgBP2 KO mice.

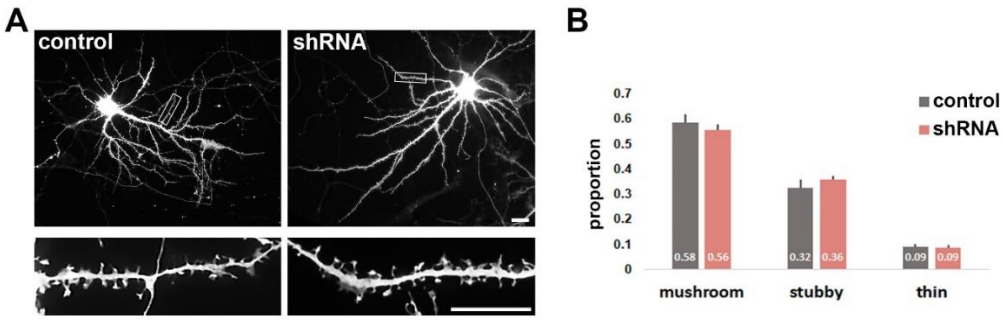

Figure 15 nArgBP2 KD does not change the ratio of population of different morphological types of spines in mature neurons.

A, Representative spine morphologies from dendrites of neurons expressing scrambled (control) or shRNA-nArgBP2. Neurons were transfected at DIV 15 and fixed at DIV 21. Lower panels are enlarged images of parts enclosed with rectangles. Scale bars; 20 μm. B, The ratio of mushroom, stubby and thin-shaped spines from control and shRNA-transfected neurons. Student's *t*-test, n=10 neurons from 3 independent cultures for control, n = 19 neurons from 3 independent cultures for nArgBP2 KD.

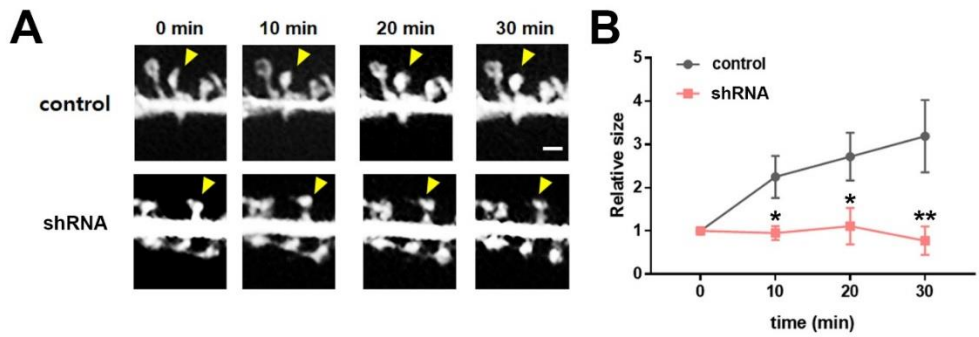

Figure 16 nArgBP2 KD inhibits spine enlargement following structural plasticity.

A, Representative images acquired at time points shown relative to the end of cLTP stimulus. Neurons were transfected with control plasmid or shRNA-nArBP2 at DIV 16 and imaged at DIV 22. Arrowheads indicate the example spines measured for analysis in each group. Scale bar; 2 μm. B, Pooled data from live imaging experiments. Spine size is normalized to the 0 min value for each group. Data are from 7 or 8 spines per condition. *$p < 0.05$, **$p < 0.01$. Error bars indicate mean ± s.e.m.

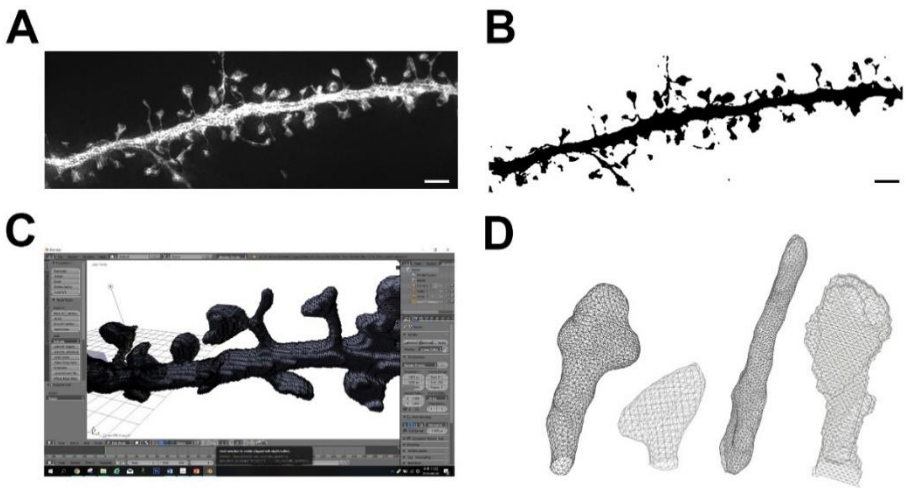

Figure 17 A method for measuring 3D geometry of dendritic spines.

A, Representative flattened images acquired with 3D-SIM. Scale bar; 5 μm. B, Binarized image of reconstructed 3D-SIM image. Scale bar; 5 μm. C, D, Detection and isolation of polygonal meshes of dendritic spines.

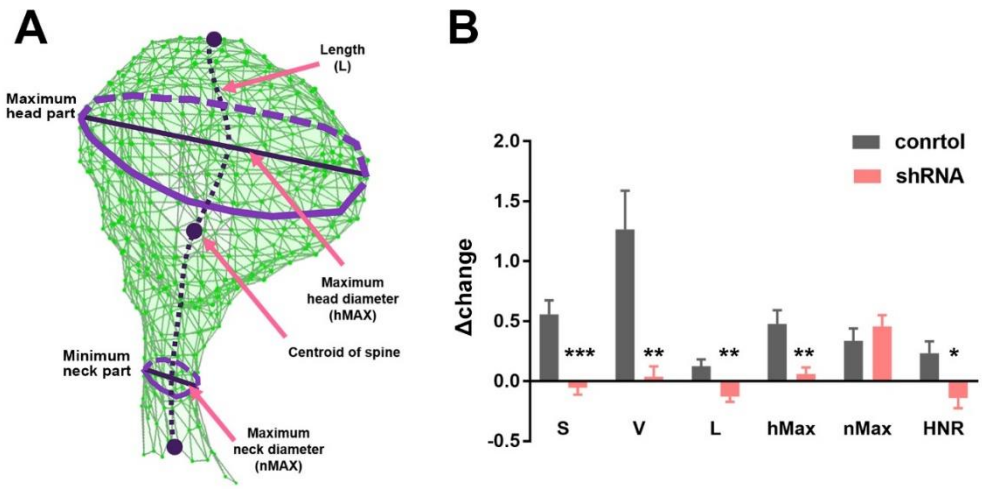

Figure 18 nArgBP2 KD inhibits morphological changes of dendritic spine following structural plasticity.

A, 3D morphological features representing the properties of the spine. B, Pooled data from 3D-SIM imaging experiments and computational measurements using custom MATLAB codes. Change values of spines are normalized to the 0 min value for each group. Data are from 38 or 32 spines per condition. S, surface area; V, volume; L, length; hMax, maximum head diameter; nMax, maximum neck diameter; HNR, head to neck ratio. *p <0.05, **p <0.01, ***p <0.001; Student's *t* test. Error bars indicate mean ± s.e.m.

Table 1 Turnover time constant of fluorescence recovery after photobleaching and percentages of stable and dynamic actin in control, nArgBP2 KD, and in nArgBP2 KD neurons treated with the Rac1 inhibitor, NSC23766.

	Turnover time (s)	% Immobile Actin $f_i \times 100$	% Mobile Actin $f_m \times 100$
control	29.99 ± 1.65	19.7 ± 1.09	80.3 ± 1.14
shRNA	28.12 ± 1.40	4.90 ± 0.54	95.1 ± 1.16
shRNA + NSC	27.59 ± 1.89	27.1 ± 1.45	72.9 ± 1.14

DISCUSSION

In this study, I demonstrate that nArgBP2 may function as a regulator of actin dynamics in dendritic spines. I showed that nArgBP2 ablation reduces the number of mushroom-shaped dendritic spines and selectively inhibits the spine-synapse formation in developing neurons. This alteration of actin dynamics correlates with the amplification of the shape factor fluctuation and the increase in the dendritic spine motility. FRAP experiment revealed that nArgBP2 KD increases the pool of dynamic actin while diminishes the amount of stable F-actin. I also showed that cLTP in nArgBP2 KD neurons could not induce normal spine head enlargement in mature neurons.

I found that the density of total dendritic protrusions is decreased and the proportion of mushroom-shaped spines is dramatically decreased with nArgBP2 KD (1). Consistent with my findings, Zhang *et al.* have also found that dendritic trees of DG granule cells in ArgBP2/nArgBP2 (*SORBS2*) KO mice show much less complexity and the number of dendritic branch points are significantly reduced (23). Therefore, reduction in the number of mushroom-shaped dendritic spines and subsequent inhibition of the spine-synapse formation that I have observed here are highly consistent with the spine phenotypes observed in individuals with BD, SCZ and ID. Thus, I believe that it could provide

the neurobiological basis that links the reduction in expression of nArgBP2 with a synaptic dysfunction associated with such disorders.

The C-terminal SH3 domains of nArgBP2 bind to WAVE 1 and 2, and to components of a WAVE regulatory complex such as PIR121 and Nap1 (4). WAVE is controlled by Rac1 with WAVE regulatory complex that stably associate with WAVE. I showed here that nArgBP2 KD increases levels of the active pool of WAVE1 (phosphor-tyrosine 151 WAVE1) (**Figure 8A**). These results are consistent with increase in the dynamic pool of spine F-actin observed in nArgBP2 KD neurons and support the previous observations that ArgBP2/nArgBP2 downregulation in astrocytes increases actin dynamics (4). I observed molecular markers of Rac1 activation in nArgBP2-depleted cells as nArgBP2 plays a global role in suppressing WAVE activation. I found that both PAK and cofilin phosphorylation are elevated in nArgBP2 KD, causing significant changes in F-actin remodeling (**Figure 8B and C**). Accordingly, either the inhibition of PAK1 or the activation of cofilin combined to sequestration of WAVE by mSH3-1/2 compensates for the ablation of nArgBP2 and rescues spine defects (**Figure 10A-E**). Besides, the inhibition of Rac1 by the treatment of neuronal cells with NSC23766, successfully rescues the phenotype of nArgBP2 KD in actin composition (**Figure 13 A-D**). The observed recovery of spine formation through the inhibition of Rac1/PAK1 pathway is explained with the ability of cofilin to balance the

burst of local polymerization of F-actin within spines, due to the over-activation of WAVE-Arp2/3 pathways. Whether functional spine-synapses are also rescued or not may provide more concrete evidence and would certainly be of interest for further study.

A recent study (28) demonstrated the physical interaction of nArgBP2 with Shank3, loss of which is associated to autism spectrum disorders. Interestingly, transgenic mice overexpressing Shank3 show a hyperkinetic neuropsychiatric-like disorder, and higher levels of Shank3 increase local accumulation of F-actin in dendritic spine through its direct effect on Arp2/3 complex (26). Thus, nArgBP2, through its action on WAVE, which is closely interconnected with Shank3, regulates local polymerization of F-actin in spine glutamatergic synapses and may play a role in several neuropsychiatric disorders. Furthermore, PIR121, which interacts with nArgBP2 SH3 domains (3), is also called cytoplasmic (fragile X mental retardation protein (FMRP) interacting protein 2 (CYFIP2) as it binds to the translational repressor FMRP that is mutated in patients affected by Fragile X syndrome (52, 53). FMRP-null neurons show a striking reduction in mushroom-shaped spines and a massive increase of actin filopodia-like structures (54), very similar to what I showed here in nArgBP2 KD neurons. nArgBP2 through its simultaneous binding to both WAVE and CYFIPs would inhibit WAVE-mediated actin polymerization and may affect local mRNA translation at the synapse,

employing a multi-step control of synapse formation and maturation.

Furthermore, I observed a very striking absence of mushroom-shaped spines in nArgBP2 KD excitatory neurons and a preferential assemble of synaptic contacts on the dendritic shafts. Although the majority of glutamatergic synapses are on spines in adult animal, the balance between spine-synapse and shaft-synapse is important to control neuronal efficacy and any alteration of this equilibrium could lead to various psychiatric disorders. Indeed, recent study showed that deletion of the autism-associated gene neurobeachin reduces the number of spinous synapses and excitatory synapses terminating at dendritic shafts instead of spines (55). Another related study showed that EphrinB3, whose signaling is also linked to anxiety disorders, autism and mental retardation, selectively promotes glutamatergic synapse formation on shaft (56). Since excitatory inhibitory (E/I) synaptic imbalance likely leads to a broad spectrum of neuropsychiatric disorders, the morphological changes in synapses of nArgBP2 KD neurons that only alter excitatory synapse formation, could lead to E/I imbalance in a certain neural circuit related to behavioral phenotypes observed in ASD and ID.

I also suggest nArgBP2 as a novel regulator of dendritic spine dynamics, both in formation of initial spine structure and in spine enlargement during

structural plasticity. Upon chemical LTP stimulus, dendritic spines continue to enlarge past 30 to 60 min, which is blocked by nArgBP2 KD. This was also confirmed by 3D-SIM imaging and measurement of 3D morphological features of dendritic spines of control and nArgBP2 KD neurons. The results suggest that nArgBP2 may be involved in the pathway that regulates actin cytoskeleton dynamics following LTP stimulation.

Spine pathology is a convergence point of many neuropsychiatric disorders, supported emerging evidence from human post-mortem, cellular, animal and genetic studies (57). Each disorder is associated with a distinct pattern of changes in dendritic spine, and altered structural plasticity of spines is proposed to be a crucial mechanism in these disorders (58). Indeed, recent studies suggest that deletion or overexpression of postsynaptic proteins such as nArgBP2, SAPAP and SHANK leads to behavioral phenotypes that are similar to symptoms observed in human neuropsychiatric diseases such as ASD, BD, SCZ and OCD (26, 59-61). Deletion of SAPAP causes OCD-like behaviors (25), and some genetic variants of SAPAP2 are associated with ASD (62) and increased SAPAP2 expression contributes to the pathogenesis of SCZ (63). In addition, Shank3 deletion or mutation is associated with ASD (64) and its duplication exhibits BD like manic behaviors (26). Other mutation in Shank3 causes SCZ-like behaviors (65). Deletion of nArgBP2 causes

ID and BD-like symptoms (23, 59). Interestingly, SHANK binds to the GH1 domain of SAPAP directly via its PDZ domain. SAPAP binds to the SH3 domain of nArgBP2 via its proline rich region. nArgBP2 and SHANK share a number of proteins as common binding partners.

Therefore, three major postsynaptic proteins that are associated with major neuropsychiatric diseases indeed interact with each other in the dendritic spines of excitatory synapses and the high incidence of comorbidities among neuropsychiatric disorders is comprehensible. Although the underlying molecular mechanisms that connect between the aberrant expression of these genes and behavioral consequences are still far from understanding, E/I imbalance caused by dysregulation of actin cytoskeleton in the dendritic spines has been suggested as a shared key molecular mechanism.

I propose a hypothesis that nArgBP2, SAPAP and SHANK form the core scaffolding triad and together regulate actin cytoskeleton in dendritic spines. Different levels of expression or activity of this core-triad may result in different phenotypes of neuropsychiatric disorders in a brain region-specific manner, thus asserting that the actin regulation by the core-triad in dendritic spines is a convergent mechanism for neuropsychiatric disorders. Like each point of equilateral triangle, these

three proteins interact with each other forming a structural and functional postsynaptic scaffold that organizes multiple protein interactions to finally regulate the actin cytoskeletons in dendritic spines. Altered expression levels or mutation status of either one or more of the core-triad proteins in a specific brain region would break the balance among the interactomes and induce the defects in actin regulation, leading to abnormalities of spine structures and subsequently to defects in the excitatory synaptic integrity. Depending on which individual protein is affected and which distinct protein network is disrupted, E/I balance may be differently altered at molecular, synaptic, and circuit levels in a brain region-specific manner, thus contributing to diverse phenotypes of mental disorders. By combining genetic approaches and recently developed imaging techniques, identifying critical brain regions and neuronal types where the core-triad protein complex of nArgBP2, SAPAP and SHANK regulates synaptic function differently will help us to test and advance this tempting hypothesis. Moreover, it will contribute to broadening the knowledge base for comorbidities and ultimately identifying new molecular targets for treatment.

References

1. Lee SE, *et al.* (2016) nArgBP2 regulates excitatory synapse formation by controlling dendritic spine morphology. *Proc Natl Acad Sci U S A* 113(24):6749-6754.
2. Kawabe H, *et al.* (1999) nArgBP2, a novel neural member of ponsin/ArgBP2/vinexin family that interacts with synapse-associated protein 90/postsynaptic density-95-associated protein (SAPAP). *The Journal of biological chemistry* 274(43):30914-30918.
3. Kioka N, Ueda K, & Amachi T (2002) Vinexin, CAP/ponsin, ArgBP2: a novel adaptor protein family regulating cytoskeletal organization and signal transduction. *Cell structure and function* 27(1):1-7.
4. Cestra G, Toomre D, Chang S, & De Camilli P (2005) The Abl/Arg substrate ArgBP2/nArgBP2 coordinates the function of multiple regulatory mechanisms converging on the actin cytoskeleton. *Proc Natl Acad Sci U S A* 102(5):1731-1736.
5. Soubeyran P, Barac A, Szymkiewicz I, & Dikic I (2003) Cbl-ArgBP2 complex mediates ubiquitination and degradation of c-Abl. *The Biochemical journal* 370(Pt 1):29-34.
6. Wang B, Golemis EA, & Kruh GD (1997) ArgBP2, a multiple Src homology 3 domain-containing, Arg/Abl-interacting protein, is phosphorylated in v-Abl-transformed cells and localized in stress fibers and cardiocyte Z-disks. *The Journal of biological chemistry* 272(28):17542-17550.

7. Haglund K, Ivankovic-Dikic I, Shimokawa N, Kruh GD, & Dikic I (2004) Recruitment of Pyk2 and Cbl to lipid rafts mediates signals important for actin reorganization in growing neurites. *Journal of cell science* 117(Pt 12):2557-2568.
8. Stradal TE, *et al.* (2004) Regulation of actin dynamics by WASP and WAVE family proteins. *Trends in cell biology* 14(6):303-311.
9. Kim Y, *et al.* (2006) Phosphorylation of WAVE1 regulates actin polymerization and dendritic spine morphology. *Nature* 442(7104):814-817.
10. Threadgill R, Bobb K, & Ghosh A (1997) Regulation of dendritic growth and remodeling by Rho, Rac, and Cdc42. *Neuron* 19(3):625-634.
11. Ridley AJ (2006) Rho GTPases and actin dynamics in membrane protrusions and vesicle trafficking. *Trends in cell biology* 16(10):522-529.
12. Sells MA & Chernoff J (1997) Emerging from the Pak: the p21-activated protein kinase family. *Trends in cell biology* 7(4):162-167.
13. Arber S, *et al.* (1998) Regulation of actin dynamics through phosphorylation of cofilin by LIM-kinase. *Nature* 393(6687):805-809.
14. Bamburg JR (1999) Proteins of the ADF/cofilin family: essential regulators of actin dynamics. *Annual review of cell and developmental biology* 15:185-230.
15. dos Remedios CG, *et al.* (2003) Actin binding proteins: regulation

of cytoskeletal microfilaments. *Physiological reviews* 83(2):433-473.

16. Hayashi ML, *et al.* (2004) Altered cortical synaptic morphology and impaired memory consolidation in forebrain- specific dominant-negative PAK transgenic mice. *Neuron* 42(5):773-787.
17. Golden SA, *et al.* (2013) Epigenetic regulation of RAC1 induces synaptic remodeling in stress disorders and depression. *Nat Med* 19(3):337-344.
18. Ramakers GJ (2002) Rho proteins, mental retardation and the cellular basis of cognition. *Trends Neurosci* 25(4):191-199.
19. Gilman SR, *et al.* (2011) Rare de novo variants associated with autism implicate a large functional network of genes involved in formation and function of synapses. *Neuron* 70(5):898-907.
20. Fromer M, *et al.* (2014) De novo mutations in schizophrenia implicate synaptic networks. *Nature* 506(7487):179-184.
21. Lein ES, *et al.* (2007) Genome-wide atlas of gene expression in the adult mouse brain. *Nature* 445(7124):168-176.
22. Strakowski SM, Delbello MP, & Adler CM (2005) The functional neuroanatomy of bipolar disorder: a review of neuroimaging findings. *Molecular psychiatry* 10(1):105-116.
23. Zhang Q, *et al.* (2016) Impaired Dendritic Development and Memory in Sorbs2 Knock-Out Mice. *The Journal of neuroscience : the official journal of the Society for Neuroscience* 36(7):2247-2260.
24. Feng G (2010) Patent US 20100077493 A1.

25. Welch JM, *et al.* (2007) Cortico-striatal synaptic defects and OCD-like behaviours in Sapap3-mutant mice. *Nature* 448(7156):894-900.
26. Han K, *et al.* (2013) SHANK3 overexpression causes manic-like behaviour with unique pharmacogenetic properties. *Nature* 503(7474):72-77.
27. Gauthier J, *et al.* (2009) Novel de novo SHANK3 mutation in autistic patients. *Am J Med Genet B Neuropsychiatr Genet* 150B(3):421-424.
28. Peca J, *et al.* (2011) Shank3 mutant mice display autistic-like behaviours and striatal dysfunction. *Nature* 472(7344):437-442.
29. Guo P, *et al.* (2012) Rapid and simplified purification of recombinant adeno-associated virus. *J Virol Methods* 183(2):139-146.
30. Zhao H, *et al.* (2014) SCAMP5 plays a critical role in synaptic vesicle endocytosis during high neuronal activity. *The Journal of neuroscience : the official journal of the Society for Neuroscience* 34(30):10085-10095.
31. Dunn KW, Kamocka MM, & McDonald JH (2011) A practical guide to evaluating colocalization in biological microscopy. *Am J Physiol Cell Physiol* 300(4):C723-742.
32. Rodriguez A, Ehlenberger DB, Dickstein DL, Hof PR, & Wearne SL (2008) Automated three-dimensional detection and shape classification of dendritic spines from fluorescence microscopy images. *PLoS One* 3(4):e1997.

33. Kashiwagi Y, *et al.* (2019) Computational geometry analysis of dendritic spines by structured illumination microscopy. *Nat Commun* 10(1):1285.
34. Zucconi A, Dente L, Santonico E, Castagnoli L, & Cesareni G (2001) Selection of ligands by panning of domain libraries displayed on phage lambda reveals new potential partners of synaptojanin 1. *J Mol Biol* 307(5):1329-1339.
35. Eden S, Rohatgi R, Podtelejnikov AV, Mann M, & Kirschner MW (2002) Mechanism of regulation of WAVE1-induced actin nucleation by Rac1 and Nck. *Nature* 418(6899):790-793.
36. Innocenti M, *et al.* (2004) Abi1 is essential for the formation and activation of a WAVE2 signalling complex. *Nat Cell Biol* 6(4):319-327.
37. Proepper C, *et al.* (2007) Abelson interacting protein 1 (Abi-1) is essential for dendrite morphogenesis and synapse formation. *EMBO J* 26(5):1397-1409.
38. Lin WH & Webb DJ (2009) Actin and Actin-Binding Proteins: Masters of Dendritic Spine Formation, Morphology, and Function. *The open neuroscience journal* 3:54-66.
39. Hotulainen P & Hoogenraad CC (2010) Actin in dendritic spines: connecting dynamics to function. *The Journal of cell biology* 189(4):619-629.
40. Zhang W & Benson DL (2001) Stages of synapse development defined by dependence on F-actin. *The Journal of neuroscience : the official journal of the Society for Neuroscience* 21(14):5169-

5181.

41. Cingolani LA & Goda Y (2008) Actin in action: the interplay between the actin cytoskeleton and synaptic efficacy. *Nature reviews. Neuroscience* 9(5):344-356.

42. Yang N, *et al.* (1998) Cofilin phosphorylation by LIM-kinase 1 and its role in Rac-mediated actin reorganization. *Nature* 393(6687):809-812.

43. Boda B, Nikonenko I, Alberi S, & Muller D (2006) Central nervous system functions of PAK protein family: from spine morphogenesis to mental retardation. *Molecular neurobiology* 34(1):67-80.

44. Nikolic M (2008) The Pak1 kinase: an important regulator of neuronal morphology and function in the developing forebrain. *Molecular neurobiology* 37(2-3):187-202.

45. Penzes P, *et al.* (2003) Rapid induction of dendritic spine morphogenesis by trans-synaptic ephrinB-EphB receptor activation of the Rho-GEF kalirin. *Neuron* 37(2):263-274.

46. Fischer M, Kaech S, Wagner U, Brinkhaus H, & Matus A (2000) Glutamate receptors regulate actin-based plasticity in dendritic spines. *Nat Neurosci* 3(9):887-894.

47. Holtmaat A & Svoboda K (2009) Experience-dependent structural synaptic plasticity in the mammalian brain. *Nature reviews. Neuroscience* 10(9):647-658.

48. Alvarez VA & Sabatini BL (2007) Anatomical and physiological plasticity of dendritic spines. *Annu Rev Neurosci* 30:79-97.

49. Zuo Y, Lin A, Chang P, & Gan WB (2005) Development of long-term dendritic spine stability in diverse regions of cerebral cortex. *Neuron* 46(2):181-189.

50. Blender (Foundation, blender. home of the blender project - free and open 3d creation software.

51. Qiao H, *et al.* (2016) Dendritic Spines in Depression: What We Learned from Animal Models. *Neural Plast*.

52. Schenck A, *et al.* (2003) CYFIP/Sra-1 controls neuronal connectivity in Drosophila and links the Rac1 GTPase pathway to the fragile X protein. *Neuron* 38(6):887-898.

53. Schenck A, Bardoni B, Moro A, Bagni C, & Mandel JL (2001) A highly conserved protein family interacting with the fragile X mental retardation protein (FMRP) and displaying selective interactions with FMRP-related proteins FXR1P and FXR2P. *Proc Natl Acad Sci U S A* 98(15):8844-8849.

54. Comery TA, *et al.* (1997) Abnormal dendritic spines in fragile X knockout mice: maturation and pruning deficits. *Proc Natl Acad Sci U S A* 94(10):5401-5404.

55. Niesmann K, *et al.* (2011) Dendritic spine formation and synaptic function require neurobeachin. *Nat Commun* 2:557.

56. Aoto J, *et al.* (2007) Postsynaptic ephrinB3 promotes shaft glutamatergic synapse formation. *The Journal of neuroscience : the official journal of the Society for Neuroscience* 27(28):7508-7519.

57. Forrest MP, Parnell E, & Penzes P (2018) Dendritic structural

plasticity and neuropsychiatric disease. *Nature reviews. Neuroscience* 19(4):215-234.

58. Penzes P, Cahill ME, Jones KA, VanLeeuwen JE, & Woolfrey KM (2011) Dendritic spine pathology in neuropsychiatric disorders. *Nat Neurosci* 14(3):285-293.

59. Feng G (2010) US20100077493 A1.

60. Ryu S, *et al.* (2011) Interaction between genetic variants of DLGAP3 and SLC1A1 affecting the risk of atypical antipsychotics-induced obsessive-compulsive symptoms. *Am J Med Genet B Neuropsychiatr Genet* 156B(8):949-959.

61. Zhou Y, *et al.* (2016) Mice with Shank3 Mutations Associated with ASD and Schizophrenia Display Both Shared and Distinct Defects. *Neuron* 89(1):147-162.

62. Pinto D, *et al.* (2010) Functional impact of global rare copy number variation in autism spectrum disorders. *Nature* 466(7304):368-372.

63. Li JM, *et al.* (2014) Role of the DLGAP2 gene encoding the SAP90/PSD-95-associated protein 2 in schizophrenia. *PLoS One* 9(1):e85373.

64. Durand CM, *et al.* (2007) Mutations in the gene encoding the synaptic scaffolding protein SHANK3 are associated with autism spectrum disorders. *Nat Genet* 39(1):25-27.

65. de Sena Cortabitarte A, *et al.* (2017) Investigation of SHANK3 in schizophrenia. *Am J Med Genet B Neuropsychiatr Genet* 174(4):390-398.

Abstract in Korean (국문초록)

수상돌기가시는 뇌에서 대부분의 흥분성 시냅스 신호를 받는 수상돌기 상의 시냅스후 특이구조이다. 수상돌기가시 구조는 주로 액틴 필라멘트로 이루어져 있으며, 액틴 골격구조는 PSD와 같은 특수구조를 포함하는 구조적 및 기능적 네트워크를 형성한다. 수상돌기가시의 형태는 매우 다양하며, PSD에 존재하는 수많은 액틴 조절 단백질들에 의해 역동적으로 조절된다.

그 발병 기작이 완전히 밝혀지지 않았지만, SAPAP 및 SHANK와 같은 시냅스후 단백질들이 양극성 장애, 자폐 스펙트럼 장애, 강박장애 및 정신분열증과 같은 다양한 형태의 기분장애에 관련되어 있음이 알려지고 있다. 최근 연구에서 수상돌기가시의 구조적 리모델링이 시냅스 가소성에 중요하며 액틴 골격구조를 조절하는 메커니즘이 신경정신질환에서 나타나는 수상돌기가시 병리에 기여할 수 있음을 시사하고 있다.

nArgBP2는 흥분성 시냅스의 형성과 기능에 중요한 시냅스후 발판단백질인 SAPAP3와 직접 상호 작용하는 단백질로 알려져 있다. 이전 연구에서 ArgBP2/nArgBP2가 액틴 골격구조를 조절하는 신호전달경로를 조정함으로써 세포의 부착과 운동성 사이의 균형을 제어함이 알려졌다. 또한 최근 연구에 따르면 쥐에서 ArgBP2/nArgBP2(SORBS2)의 유전적 결실은 인간의 지적 장애 (ID)와 유사한 행동을 유발하는 것으로 알려졌다. 하지만

nArgBP2의 결핍이 어떻게 지적장애의 증상을 나타내게 되는지, nArgBP2가 시냅스에서 어떻게 작용하여 지적장애를 유발하는 세포 및 분자적 메커니즘에 영향을 주는지에 대해 완전히 알려지지 않았다.

이전 연구의 결과를 바탕으로 시냅스에서 nArgBP2의 역할을 규명하기 위해 다음과 같이 가설을 설정하였다. 1)nArgBP2는 시냅스후세포에서 액틴 골격구조를 조절하는 주요 단백질 중 하나이며, 2) nArgBP2는 수상돌기가시의 형태변화를 조절하고, 3) 수상돌기가시는 대부분의 흥분성 신호를 받는 특이구조이므로 nArgBP2가 흥분성 시냅스의 형성을 조절할 것이며, 4) 흥분-억제성 시냅스의 균형 (E/I 균형)이 신경계의 항상성 기능을 유지하는 중요기 때문에, nArgBP2 결핍으로 인한 E/I 불균형이 지적장애에서 관찰되는 시냅스 이상과 관련된 근본적인 요인일 수 있다.

RNA 간섭에 의한 nArgBP2의 발현 저해는 수상돌기가시 형성에 영향을 주어 정상적인 형태가 아닌 필로포디아(filopodia)의 형성을 증가시켰다. 또한 정상적인 수상돌기가시 형성의 결함은 억제성 시냅스 형성에 영향이 없었던 반면, 흥분성 시냅스가 수상돌기가시 말단이 아닌 수상돌기 축에 형성됨을 발견하였다. 흥분성 시냅스의 이상은 미니어처 흥분성 시냅스 후 전류의 평균 빈도를 감소시켰다.

nArgBP2가 저해된 신경세포에서 수상돌기가시의 형태변화는 WAVE1/PAK/cofilin의 인산화와 관련이 있으며, WAVE와의 상호작용이 저해된 상태에서 PAK을 억제하거나 cofilin을 활성화시킴으로써 nArgBP2 저해 효과가 상쇄됨을 발견하였다. 또한 실시간세포영상기법을 이용하여

nArgBP2의 기능이 저해된 발달 단계의 신경세포에서 액틴골격 역학의 현저한 증가가 수상돌기가시의 운동성을 크게 증가시킴을 확인하였다.

놀랍게도, 신경세포의 수상돌기가시가 형성되어 안정화된 후인 성숙단계에서는 nArgBP2의 발현 저해로 인한 수상돌기가시 형태의 결함이 발견되지 않았다. 발달단계의 신경세포와 같이 구조적 리모델링이 일어날 때 nArgBP2가 필요할 수 있을 것이라고 추론하였고, 이를 확인하기 위해 성숙한 신경세포의 새로운 시냅스 형성을 일으키는 화학적 장기 강화(cLTP: chemical long-term potentiation)를 유도해보았다. 화학적 장기 강화는 성숙단계의 뉴런에서 시냅스 전-후 구조의 리모델링을 포함하여 발달 단계에서 나타나는 현상들을 모방하는 것으로 알려져 있다. 화학적 장기 강화를 일으켰을 때 컨트롤 세포의 수상돌기가시는 그 크기가 커지는 반면 nArgBP2의 발현이 저해된 신경세포에서는 크기가 변하지 않거나 작아지는 현상을 발견하였다. 이는 같은 조건에서 초고해상도 이미징을 통한 3 차원 구조의 형태학적 측정값을 확인한 결과, nArgBP2의 결핍이 수상돌기가시의 머리크기 확대를 저해함을 발견하였다. 이러한 결과는 nArgBP2가 성숙한 뉴런에서도 액틴 골격의 역학을 조절한다는 가설을 뒷받침할 수 있다.

종합해보면, 이 연구는 nArgBP2가 수상돌기가시에서 액틴 골격구조의 활동성을 조절하는 기능을 담당함을 밝혔다. 또한 nArgBP2가 신경세포의 발달단계에서 수상돌기가시 형성 및 스파인-시냅스 형성, 성숙단계에서 시냅스 가소성과 같은 동적인 액틴 구조 리모델링이 일어날 때 특히 중요한

역할을 함을 확인하였다. nArgBP2 발현 감소로 인한 시냅스 액틴 골격구조의 비정상적인 조절이 지적 장애에서 관찰되는 시냅스 E/I 불균형에 기여할 수 있을 것으로 사료된다.

* 본 내용은 *PNAS*에 출판 완료된 내용임 (1).

.....

주요어 : nArgBP2, 수상돌기가시, 액틴 골격구조, 흥분성 시냅스, 화학적 장기 강화, 흥분성/억제성 균형

학 번 : 2013-23532